8-2020

Fluted Films Caused by Gravity Driven Water Drainage from Vertical Tubes

Matthew B. Jones
Utah State University

FLUTED FILMS CAUSED BY GRAVITY DRIVEN WATER DRAINAGE FROM VERTICAL TUBES

by

Matthew B. Jones

A proposal submitted in partial fulfillment
of the requirements for the degree

of

MASTER OF SCIENCE

in

Mechanical Engineering

Approved:

Tadd T. Truscott, Ph.D. Major Professor	Som Dutta, Ph.D. Committee Member
Hailei Wang, Ph.D. Committee Member	Richard S. Inouye, Ph.D. Vice Provost for Graduate Studies

UTAH STATE UNIVERSITY
Logan, Utah

2020

ABSTRACT

Fluted Films Caused by Gravity Driven Water Drainage from Vertical Tubes

by

Matthew B. Jones

Utah State University, 2020

Major Professor: Tadd T. Truscott, Ph.D.
Department: Mechanical and Aerospace Engineering

When a stationary mass of water in a vertical tube is suddenly released, it creates a variety of artistic shapes and behaviors as it escapes the tube exit. As the descending water accelerates in the tube, shear stress along the tube wall slows the outer radius, resulting in a transient film entrained on the tube that trails the main body of water. When this film exits the tube, surface tension, gravity, and inertia interact to cause the film to create a wide variety of shapes, including jets, tubes, water bells, champagne glasses, and bubbles; rich forms that appear in other natural realizations of thin film dynamics. Despite the seeming simplicity and ubiquity of a water column exiting a vertical tube, this transient and beautiful phenomenon has never been described or studied. Here we show how and why the varied shapes trailing the column arise using both experimental data and theoretical modelling. We found that the forms observed are the result of a highly variable exiting film state, which arises from the interaction of several distinct phenomena occurring inside the tube. The continually evolving velocity profile of the accelerating water mass, development of newly formed film, and creation of surface tension waves as the film matures all contribute to a varying film profile. Theoretical predictions that are in agreement with experiments reveal how the ultimate shape, size and breakup point of the exiting film depend on the film thickness and velocity profile at the tube outlet. We anticipate that our research will

provide a foundation for future studies involving the dynamics of falling water columns and films over a large range of physical scales and fluid properties. Furthermore, our results demonstrate how multiple known natural phenomena can interact unexpectedly to form artistically beautiful results. In this way, our work connects scientific and artistic fields, lending understanding to appreciate or create beautiful liquid shapes for fountains and other works of art.

(74 pages)

PUBLIC ABSTRACT

Fluted Films Caused by Gravity Driven Water Drainage from Vertical Tubes

Matthew B. Jones

When a stationary mass of water in a vertical tube is suddenly released, it creates a variety of artistic shapes and behaviors as it escapes the tube exit. As the descending water accelerates in the tube, friction along the tube wall slows the outer radius, resulting in a moving film entrained on the tube that trails the main body of water. When this film exits the tube, surface tension, gravity, and inertia interact to cause the film to create a wide variety of shapes, including jets, tubes, water bells, champagne glasses, and bubbles; rich forms that appear in other natural realizations of thin film dynamics. Despite the seeming simplicity and ubiquity of a water column exiting a vertical tube, this transient and beautiful phenomenon has never been described or studied. Here we show how and why the varied shapes trailing the column arise using both experimental data and theoretical modelling. We found that the forms observed are the result of a highly variable exiting film, which arises from the interaction of several distinct phenomena occurring inside the tube. These include the accelerating draining film and the development of waves on the film over time, both of which lead to a very variable exiting film. Theoretical predictions that are in agreement with experiments reveal how the ultimate shape, size and breakup point of the exiting film depend on the film thickness and velocity profile at the tube outlet. We anticipate that our research will provide a foundation for future studies involving the dynamics of falling water columns and films over a large range of physical scales and fluid properties. Furthermore, our results demonstrate how multiple known natural phenomena can interact unexpectedly to form artistically beautiful results. In this way, our work connects scientific and artistic fields, lending understanding to appreciate or create beautiful liquid shapes for fountains and other works of art.

ACKNOWLEDGMENTS

I thank my mentor, Professor Tadd Truscott of USU, for his guidance and instruction. His insights and extensive knowledge have been invaluable in guiding me through my research in general and this project in particular. Thanks also to Dr. Nathan Speirs, who discovered the fluted film phenomenon that I based my thesis on.

I would like to thank the MAE department of USU in general and Professor Barton Smith in particular for their instruction and guidance in my education. They have given me the tools I need to successfully complete this thesis and be successful in my future career. Thanks as well to the funding that I received for my research from the Office of Naval Research, Navy Undersea Research Program (Grant # N000141812334), monitored by Ms. Maria Medeiros.

Thanks to my beloved wife Emily for her encouragement, patience, sacrifice and support though this project and through my graduate education overall. She is the most important part of my life and I could not have accomplished this without her. I also thank my parents, who encouraged me to become all that I could and to reach my potential.

Finally, I thank God, my Heavenly Father, who has blessed me with my faculties and is the source of all light and knowledge.

Matthew Jones

CONTENTS

Page

LIST OF FIGURES

CHAPTER 1

INTRODUCTION

This thesis project focuses on the exit behavior of water when suddenly allowed to drain from a vertical, open-topped tube, known as "fluted film" behavior. This behavior touches on three different areas of study: water acceleration in pipes, entrained film behavior on vertical surfaces, and the behavior of axisymmetric thin liquid sheets. The phenomena can be summarized by Figure 1.1, where water of height 7.62cm in a 1.9cm inner diameter tube is released from rest. As the water accelerates through the tube (t = 80ms), it develops a curved velocity profile due to shear stress with the wall, with water travelling far slower near the tube wall than in the center. This slower travelling water is left behind the main water body, forming a thin travelling film entrained on the tube wall. This film emerges from the tube attached to the top of the water column (t = 125ms). The tubular film shrinks in diameter as it falls (t = 150ms) due to surface tension, until it finally pinches off into a jet (t = 160-170ms), in a shape reminiscent of a champagne glass and stem. The film emerging from the tube exit grows steadily thinner and slower until it no longer has enough inertia to remain stable. At this point, the film ruptures at the tube exit (t = 185ms) and disintegrates the champagne glass (t = 200ms).

This phenomenon was discovered by chance when Dr. Nathan Speirs happened to notice the film behavior while performing other research involving draining liquid in a tube (1). The phenomenon was described briefly in the poster (2), which coined the behavior's name, "fluted film". This study represents the first in-depth investigation into the fluted

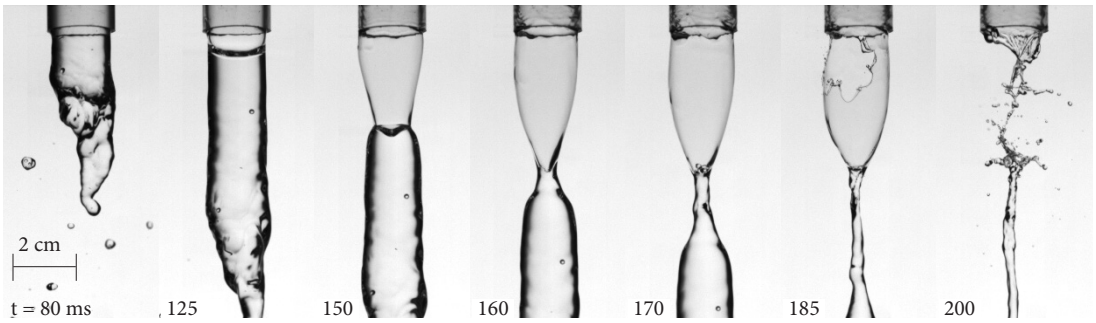

Fig. 1.1: Typical behavior seen when water exits a suddenly opened tube. The main water column exits the tube (80-125ms), with a thin tubular film trailing behind. The film diameter shrinks as it descends (150ms) until it pinches off into a jet (160-170ms), forming a champagne glass shape. The film eventually ruptures at the tube exit (185ms) and disintegrates (200ms). The 1.9cm inner diameter tube had an initial water fill height of 7.62cm.

film phenomenon.

In order to explore the exit fluted film behavior of water as it drains out of a tube, it is necessary to first understand the evolving velocity profile of water prior to tube exit. The velocity profile of fully-developed water flow in pipes is relatively straightforward and can be readily derived (3). However, the developing profile of an accelerating liquid starting at rest is far more complex. Szymanski(4) derived an analytical solution for pipe flow driven from rest by a steady pressure gradient. This solution describes how the velocity develops across the radius over time. This solution has been experimentally verified by Lefebvre and LaPointe(5) and Lefebvre(6), and compares well with other models (7). It is used as the foundation of modern unsteady laminar pipe flow research, and is used in this study. Though the solution is pressure-driven instead of gravity-driven, the development of the flow over time for both flows is the same and the derivation of a model for both use the same technique.

The formation and development of films entrained on surfaces is another integral part

of the study. This field is divided into two subcategories: withdrawal and drainage. Withdrawal involves the formation of a film when an object is withdrawn from a stationary liquid bath (Landau and Levich(8), Levich(9), etc.), while drainage film formation occurs when a liquid, initially at rest, drains off of a vertical surface (10). This study is concerned with the second kind, as the tubes used are stationary with the water draining out the bottom. Jeffreys(11) laid foundational work in the field by developing an equation of film thickness as a function of time and distance from the liquid starting point, known as the Jeffrey's equation. The equation neglects inertial terms, which is valid only when either inertial forces are small relative to viscous and gravitational forces, or after a great deal of time has passed. The equation also assumes that the water starts from rest and drains from a vertical, flat surface. A similar equation for the inside of a curved cylinder was developed by Gutfinger and Tallmadge(12). Work by van Rossum(13) showed under what conditions a radius is large enough to be approximated as a flat plate, using the Goucher number (14). Van Rossum's work on a flat plate was adapted by Ali(15) to cylindrical coordinates to estimate the drainage of viscous fluids. Inertial terms in a continual flat film were incorporated by Green(16) and Wyllie(17). Their work was used in an attempt to incorporate inertial terms in a drainage film was made by Gutfinger and Tallmadge(12), which was included in the review by Tallmadge(10). However, the solution omitted a vital term and was incorrect. A corrected solution was completed by Annapurna and Ramanaiah(18), though they incorrectly determined that their solution, when time approaches infinity, contradicted the Jeffrey's equation. Roy(19) found an alternative approach to incorporating inertia by numerically solving similarity variable velocity profiles derived from the Navier-Stokes equations. Denson(20), Lang and Tallmadge(21), and de Kee(22) incorporated an

initial starting profile for post-withdrawal drainage. For large cylinder cases (as determined by van Rossum(13)), the flat plate drainage derived by Annapurna and Ramanaiah(18) is used to model the draining film thickness and velocity profile. Initial starting profiles do not need to be incorporated, as the liquid begins as a horizontal bath at rest. For the smaller cylinder cases, the work of Gutfinger and Tallmadge(12) is used to determine what film thicknesses are appropriate to continue to model using Annapurna's model. Above these thicknesses, the film is relatively close to the falling water column, and so the velocity and top film profiles created by the accelerating water column are used.

Kapitza and Kapitza(23) were the first to study in depth the waviness that develops on films flowing down a solid surface. As the film descends, tiny disturbances in the film surface slowly grow due to surface tension. This phenomenon is called the Plateau-Rayleigh instability, which is also the cause of falling water streams eventually breaking up into droplets. These growing disturbances eventually form waves. The waves are initially highly irregular, but over time develop a somewhat more consistent frequency, shape, and height, though they are far from uniform. There are many numerical models that simulate this phenomenon, such as Camassa et al.(24), Ogrosky(25), Muñoz-Cobo et al.(26), and Nguyen and Balakotaiah(27), to name a few. Unfortunately, these types of models are extremely complex and computationally expensive. For the scope of this study, a robust idea of the typical wave height, speed, and frequency over time is sufficient. Most empirical characterization studies focus on film after it has been relatively well developed, such as Koizumi et al.(28) and (29). However, a small number of empirical studies exist for the early stages of film development with parameters relevant to this study. Takahama and Kato(30) and Takamasa and Kobayashi(31) performed detailed analysis and collected empirical data

on the development of water films over time. Based on their collected data, models are contrived that predict the film's maximum and minimum heights, as well as the dominant wave frequency over time.

The final field that must be understood in this study is that of water bells. Water bells are axisymmetric film sheets that generally expand radially outward, then fall and contract inwards due to gravity and surface tension until coming in contact with either quiescent water or a cylinder, forming a sealed, bell-shaped structure. Most water bells are created by a jet impinging on either an axisymmetric surface or another jet travelling in the opposite direction. Water bells were first described by Savart(32; 33; 34), and possibly independently later on by Bourdon(35). Initial analytical descriptions modelling by balancing surface tension, inertia, and gravity was performed by Boussinesq(36; 37). These equations were used with water bells (or "wasserglocken"(38)) to find the surface tension of different liquids at various temperatures, such as water Buchwald(39; 40) and mercury Puls(41). Hopwood(42) discovered that new water bell shapes could be created by creating an air pressure difference between the entrapped air and the air outside of the bell, which would expand or contract the bell and create novel shapes. Lance and Perry(43) explained these novels shapes by numerically solving the motion equation of Boussinesq. Taylor(44) found an analytical solution to the problem when gravity was negligible and incorporated air drag into the problem. He also found the disintegration point of a thin liquid film (45), which dictates when the water bell will rupture and break. Parlange(46) incorporated the circulating air movement that eventually develops within the water bell. Water bells that are initially projected upward instead of downward or horizontal was investigated by Dumbleton(47). Clanet(48; 49) answered several questions about water bells, including the

stability (demonstrated by Aristoff et al.(50)), the dynamics of bell formation, and the ejection angle of the jet from the disk. New versions of water bells have also been investigated, such as the transonic water bells created by Brunet et al.(51), where the speed of the film equalled the speed of surface waves. Another new type of water bell was discovered by Jameson et al. and Button et al.(52; 53), where the film forms from a radially expanding fluid entrained below a horizontal surface, which eventually falls off abruptly. The original equations of motion derived by Boussinesq have proved valid throughout the history of water bell study and continue to be used. Because of this, his equations of motion are utilized, using the numerical solution laid out by Lance. Further developments in water bell theory, while useful, are not relevant to this study, as gravity is not insignificant, the water bells are initially projected downwards, and the water bells are not transonic.

Herein, a model of the exit behaviors of water draining from a tube is formalized through the use of theories described above. The developing velocity profile of the main water column is used as a starting point for film formation entrained on the tube wall. This film will develop waves and eventually exit the tube, whereupon it will form a vertically projected water bell, known as a fluted film. The shape, behavior, size, and terminus mode of the water bell will depend on the interaction of all of these phenomena. The work is validated by an extensive experimental study, wherein each of the theoretical constructs is tested. Tubes of varying size and fluid levels are used to unravel the behavior and emphasize the varied and beautiful shapes that can form.

CHAPTER 2

EXPERIMENTAL SETUP

Eight poly-carbonate tubes with inner diameters ranging from 0.3175 cm to 6.985 cm were used in the test. Water in these tubes ranges in fill height from one quarter of the tube's inner diameter up to 1.22 m (the maximum height of the tube).

The poly-carbonate tubes are cleaned before each test. The tubes are always handled with gloves prior to and during testing to prevent contamination of the tube exit from grease or oils found on the hands. Deionized water is first run through the inside of the tube to eliminate any dust. The lower opening of the tube is then wiped dry using a clean paper towel. Another paper towel soaked in isopropyl alcohol is then used to wipe away any grease or oils from fingerprints. The alcohol is allowed to dry.

Once the tube is properly cleaned, the tube is secured vertically to a stand using zip ties. Strips of rubber are placed between the zip ties and tube prior to tightening to prevent the tubes from slipping. A level is used to ensure that the tube is vertical. An inflated balloon is then wedged between the tube's bottom opening and small side supports, forming a temporary seal (Figure 2.1).

Deionized water is then poured into the tube from above until a desired fill height is reached. Fill height is the distance between the bottom opening of the tube and the bottom of the water's meniscus. Water must be poured slowly to prevent bubbles.

Any bubbles found in the water column can be removed by tapping the tube. This fill method works well for all the tubes except for the smallest tube (0.3175 cm inner diameter),

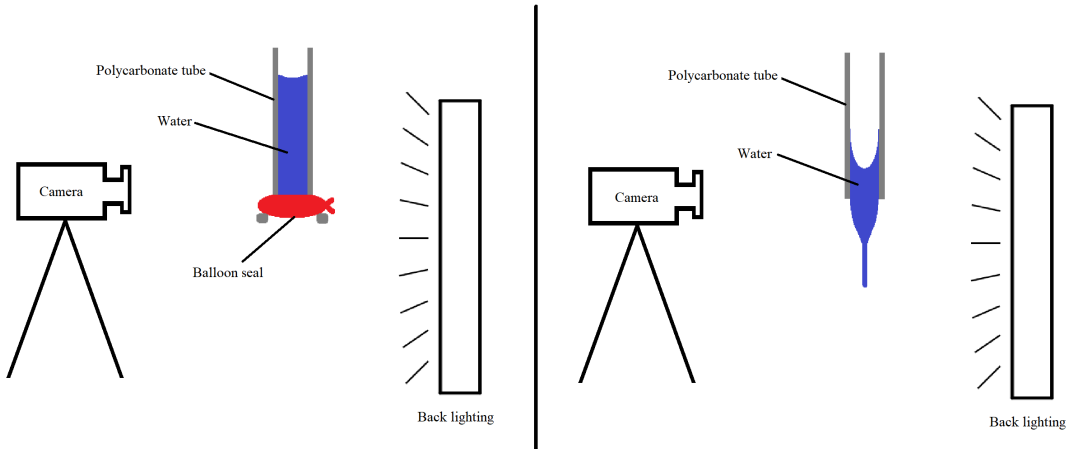

Fig. 2.1: Experimental setup, both prior to water drop (left) and during water drop (right). Prior to water drop, a polycarbonate tube partially filled with water is sealed from below with an inflated air balloon wedged between the tube exit and two metal balloon supports. When the balloon is popped, water in the polycarbonate tube is allowed to fall out of the tube. This movement is captured using a high-speed camera and back-lit using a light bank. The balloon supports are not in the camera field of view, and so are not shown in the right figure.

which must be filled from the bottom instead of the top. It is only slight larger than the water capillary length, any trapped bubbles during top filling separate all water above and below, forming air pockets that cannot be removed. Instead, the smallest tube is placed into a cup of water and the water is pulled up into the tube by capillarity. The top of the tube is then sealed, the cup removed, and then sealed with the balloon from below. The top seal is then removed.

In order to release the water, the balloon is popped. A small amount of water leaves the bottom of the tube with the balloon, but not enough to noticeably alter the fill height. The shock wave of the popping balloon sometimes disturbs the water in the tube slightly. However, this disruption dissipates before any water movement occurs in all but the lowest fill height cases, and was not judged impactful enough to affect the results in a meaningful way.

The water behavior is captured using a Photron SA3 high-speed camera with a 50 mm lens recording at 2000 frames a second. A light bank is positioned in the background in order to provide proper lighting (Figure 2.1). The camera is positioned and focused such that the tube bottom opening is near the top of the camera field of view. Once the camera is positioned and focused, length calibration is performed. This is done by first filming a ruler positioned vertically beneath the tube center. The number of pixels between ruler tick marks coincides with the lengths displayed on the ruler. This length calibration is performed whenever a new tube was installed and whenever the camera is moved.

CHAPTER 3

EXPERIMENTAL RESULTS

By varying the tube diameter and water fill height, ten different behaviors can be seen. Typical examples of each behavior can be seen in figure 3.1. Figure 3.2 shows the behaviors as a function of tube diameter and water fill height, with the letter labels corresponding to those in figure 3.1. Most behaviors are distinct and easy to identify. However, a few behaviors transition smoothly from one case to another, so the boundary between the two can be somewhat arbitrary. A description and the different behaviors and the distinction criteria is outlined below.

3.1 Static Slug

In the smallest diameter tubes with low fill height, no water exits the tube (Figure 3.1a). This is called the *Static slug* behavior. When the water is released, there is some small initial movement as the water descends enough to form a concave bulge out of the bottom of the tube. Once this bulge has ceased growing, the water column remains entirely suspended in the tube and movement ceases. The final shape of the water column entails an upper convex meniscus and lower concave bulge.

3.2 Jet

Increasing the fill height or diameter of the tube slightly from those that exhibit the *Static slug* behavior causes the water to exhibit a different behavior, called the *Jet* behavior.

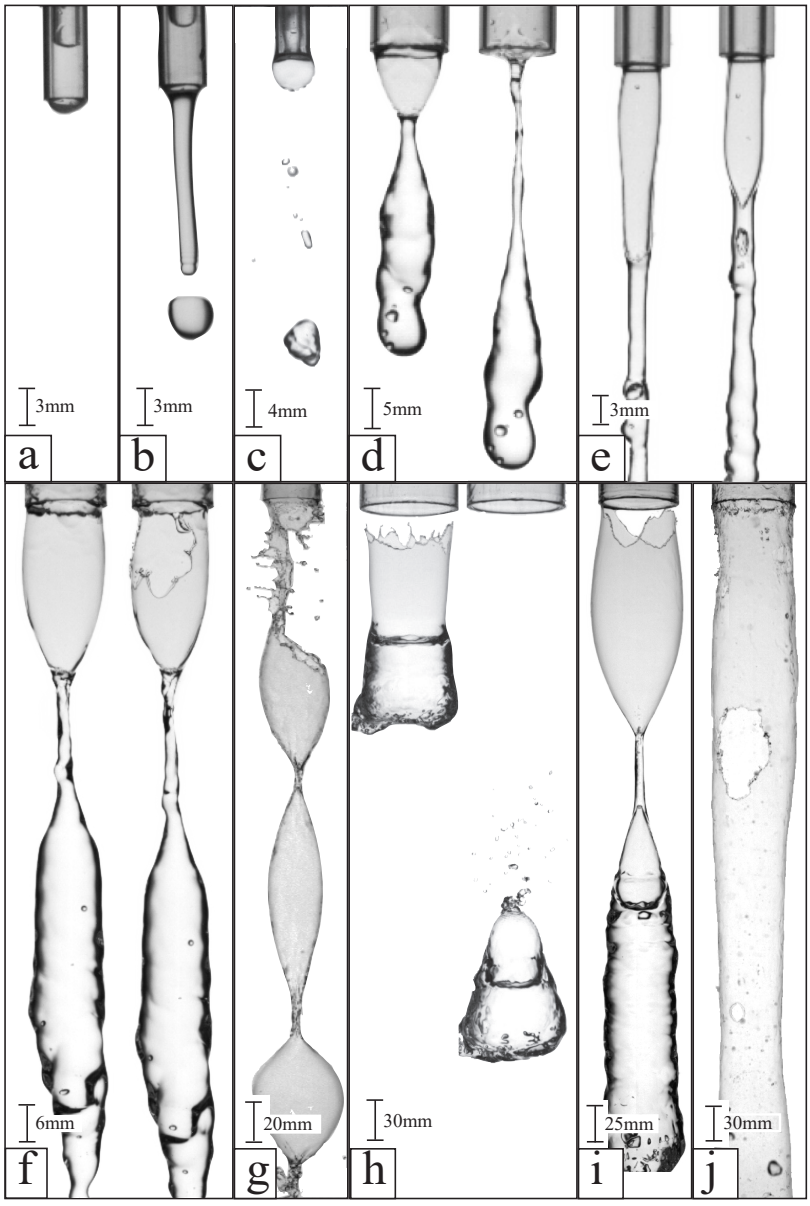

Fig. 3.1: Regimes in the observed experiments. (a) *Static slug*, with all water remaining in tube. (b) *Jet*, with some water escaping tube and the rest of the water remaining in the tube. (c) *Multiple slugs*, with a series of water slugs pushing air out of the tube, inflating bubbles created by the exit of preceding water slugs. (d) *Retracting champagne*, with a conical film reminiscent of a champagne glass (left), which recedes steadily up into the tube exit (right). (e) *Jumping champagne*, with a conical film reminiscent of a champagne glass, with the pinchoff point periodically jumping closer to the tube, before receding into the tube exit. (f) *Breaking champagne*, with a conical film reminiscent of a champagne glass (left), which eventually ruptures (right). (g) *Bubble*, with a tubular film pinching off in multiple locations, forming bubbles. (h) *Crown and bell*, with a tubular film detaching from the tube exit prior to pinchoff. (i) *Symmetric champagne*, with a film pinching off above the water column, forming a champagne shape above the pinchoff jet while trapping a conical bubble below the pinchoff jet. (j) *Tube*, with a long, tubular film breaking up before the film is able to pinch off into a jet.

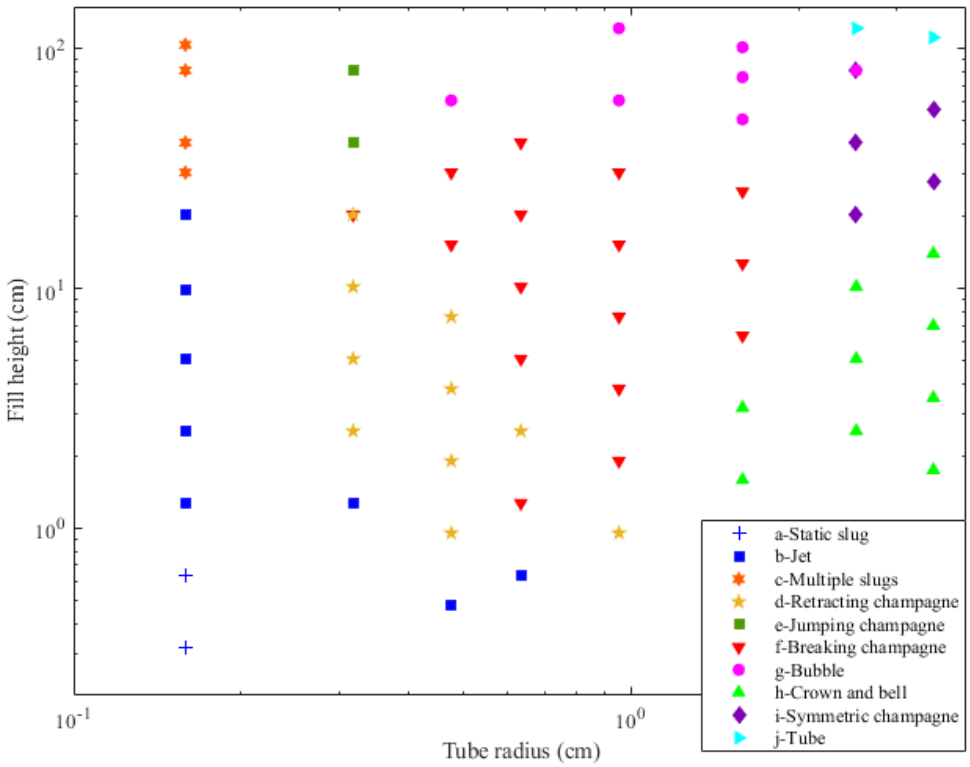

Fig. 3.2: Behavior regime diagram as a function of tube diameter and initial water fill height. Ten regimes are observed. The letters preceding the regime names correspond to the letters labeling the pictures in Figure 3.1.

In this case, some water falls down and then exits the tube in a solid jet (Figure 3.1b). However, the water still in the tube eventually slows and stops, leaving a small column of water suspended in the tube, equal to or smaller than the maximum fill height seen in the *Static slug* case.

3.3 Multiple Slugs

The *Multiple slug* behavior is different than the other external film behaviors. In the other external film cases, the main falling water column is followed by a film entrained on the tube wall. However, in the *Multiple slug* case the main water column is followed by a series of water slugs separated by air pockets (Figure 3.1c). The air pockets have water films entrained on the tube walls. The exiting water slugs and descending water films create a series of bubbles attached to the tube exit that are repeatedly inflated by the exiting air pockets and then either destroyed by over-inflation or separated from the tube by succeeding water slugs. This behavior occurs in high fill cases of the smallest tube.

3.4 Champagne Glass

As the tube diameter and fill height increase further, the entire water column falls out of the tube. Trailing behind the main water column is a film of water against the tube walls. When the film exits the tube, initially in the shape of a tube, it collapses radially inward as it descends, eventually pinching into a stream (Figure 1.1). The shape of the inwardly collapsing film resembles that of a champagne glass, hence the *Champagne Glass* name of the behavior. Once the shape has been established, one of several behaviors can be observed.

3.4.1 Retracting and Jumping Champagne Behaviors

One behavior, observed at relatively small to moderate tube size and fill heights, entails the pinch-off point of the film steadily rising until it nears the tube exit, whereupon it will rapidly recede into the tube, forming a horizontal film across the tube bottom. This behavior is known as *Retracting champagne* (Figure 3.1d). Increasing high fill height results in the *Jumping champagne* behavior, where instead of a steady rise closer to the tube, the pinch-off point periodically 'jumps' closer to the tube exit, before eventually receding into the tube exit (Figure 3.1e).

3.4.2 Breaking Champagne Behavior

Increasing the tube diameter at small to moderate fill heights creates a new *Champagne* behavior, known as *Breaking champagne*. In this behavior, the film will not retract into the tube exit, but will instead rupture and disintegrate, seen in Figure 3.1f. The rupture nearly always occurs at the tube exit, and quickly expands across the entirety of the film, until the whole thing has been disintegrated into small droplets.

3.5 Bubble

For moderately sized tubes at high fill heights, multiple pinchoff locations of the film are observed. A champagne glass shape is formed between the tube and nearest pinchoff point, but the lower pinchoff points form bubbles. Single or multiple bubbles can be observed, depending on how soon the film begins to rupture (Figure 3.1g).

3.6 Crown and Bell

For larger tube diameter cases, the water exhibits different behaviors. Water falls

through the tube and creates a film as the main slug descends, much as in the Champagne cases. However, the large amount of mass in the slug of water and large distance required for pinch-off means that the falling water slug creates a sort of base that never collapses into a stream. In the lowest fill height cases, the film quickly breaks before it pinches off, making a crown shape on top of the water slug. The film pinches off, sometimes forming a thick bubble in the water slug. These cases are labeled *Crown and bell* (Figure 3.1h).

3.7 Symmetric Champagne Glass

The *Symmetric Champagne* behavior is very similar to the *Breaking champagne* mode (Figure 3.1j). The only difference is that the film's initial pinch-off point is above the top of the main slug of water. The air trapped below the pinch point resembles an upside-down champagne glass.

3.8 Tube

In the largest tubes with the highest fill height, water falls and creates an external film, as in the other cases. However, the film never pinches off. Instead, the film breaks up before pinch-off, with the film in a somewhat conical cylinder. This breakup often occurs in multiple places at once and is called *Tube* (Figure 3.1j).

CHAPTER 4

MODEL

The varied water behavior seen when water of fill height H in tube of inner radius R (Figure 4.1a) is due to the interaction of several phenomena. Gravity, surface tension, capillary forces, viscosity, momentum, and pressure all play important roles in the observed experiments (Figure 4.2). Some combinations of the water fill height and tube diameter result in one force dominating over all the others, while others lead to an interaction of multiple different factors. These can be explained using a number of equations and models.

4.1 Trivial Cases

The most interesting and varied results come from cases that involve external tubular films coming out of the tube. These are the cases that constitute the main focus of the study. However, the two trivial cases that do not involve external films will be discussed first, namely the *Static slug* and *Jet* cases.

4.1.1 Static Slug

Immediately upon the water's release, before any movement has occurred, there are two initial forces that come into play, (Figure 4.2a). One force is gravity, which pulls the water downwards and out of the tube, while the other is capillary force, which pulls the water in the opposite direction. These capillary forces are caused by adhesion between the water and the tube, known as wetting. This interaction occurs on both the top and bottom

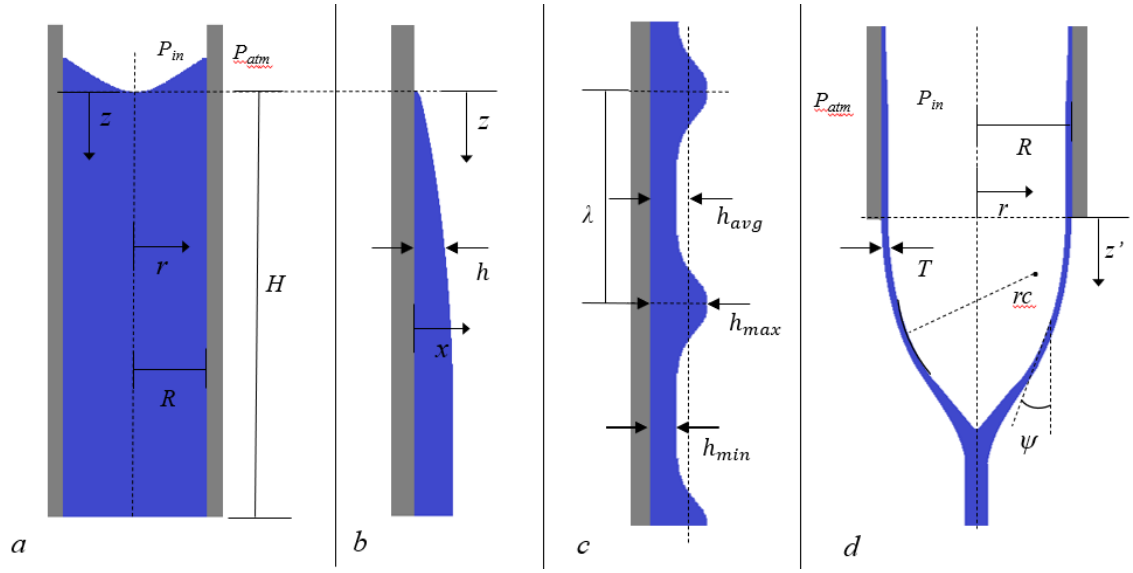

Fig. 4.1: Coordinate systems and variables defined. (a) Cylindrical coordinate system and variables used in water velocity calculations. (b) Cartesian coordinates and variables used in flat plate film drainage calculations. (c) Wave amplitude and thicknesses variables on film. (d) Cylindrical coordinates and variables used in water bell calculations

surfaces of the water column.

The relative strength of these forces can be readily derived using the Young-Laplace formula, the hydrostatic pressure formula, and the force conservation equation. The result is a modified Bond number very similar to Jurin's law

$$Bo_{mod} = \frac{2\sigma\left(cos(\theta) + sin(\theta)\right)}{\rho g R H}, \tag{4.1}$$

where σ is surface tension, θ is the static wetting angle between water and polycarbonate defined by Petke and Ray(54) and Terpilowski et al.(55), ρ is density of water, g is the acceleration due to gravity, R is the inner diameter of the tube, and H is the initial height of water in the tube prior to release.

When this number is greater than unity, capillary forces overcome gravitational forces, and the water does not exit the tube. This results in the *Static slug* behavior observed in

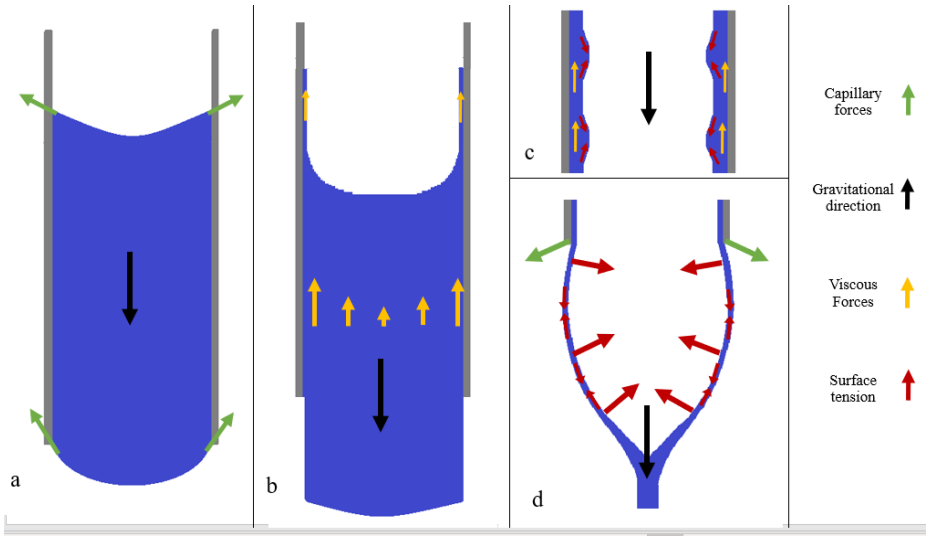

Fig. 4.2: Forces acting on water at various stages after release. (a) Forces immediately after release. Gravity pulls the water column downward, while capillary forces at the top and bottom surfaces create an upward force. (b) Forces acting on the main water column while travelling down the tube. Gravity continues to pull the water downwards, while forces slow the water near the tube wall, leaving behind a film. The force that viscosity exerts on the water column depend on how long the water has been falling. In this image, the velocity profile is still developing, and so viscosity has a low effect on the water center. (c) Forces acting on film entrained on tube. The entrained film continues draining downward due to gravity, slowed by viscosity. Surface tension and the Plateau-Rayleigh instability on the film surface causes the film to become wavy with time. (d) Forces acting on external film. Upon exit, capillary attraction between the water and tube exit cause the film to travel slightly outward as it falls. Surface tension forces due to the curvature of the film collapses the film into a jet as it falls. Surface tension also pulls the film in on itself, which can result in the film disintegrating into droplets.

figure 3.1a.

4.1.2 Jet

If Equation 4.1 is less than unity, gravity initially overcomes surface tension and at least some water will exit the tube. As water begins to exit, leaving less mass inside of the tube, it is possible for surface tension fores to eventually slow down and stop the remaining water. This is known as the *Jet* behavior observed in figure 3.1b. To stop at least some water in the tube from exiting, surface tension forces have to overcome both the gravitational pull of the remaining water and the momentum that the water has already achieved. It is useful to know under what conditions the *Jet* behavior will occur. Using the same equations employed to find Equation 4.1, as well as Newton's Second Law, $F = ma$, the acceleration of the fluid at a given tube radius and water height can be expressed as

$$a_z(z) = g - \frac{2\sigma}{\rho R(H - z)}. \tag{4.2}$$

This acceleration ignores the effects of viscosity and assumes that the center of the water tube is travelling according to the kinematic equation $u = \sqrt{2gz}$. Water has a relatively low viscosity, so this assumption should hold except for the smallest tube diameters at high fill heights. In this region, the predicted acceleration should be higher than the actual acceleration. Therefore, the predicted maximum fill height that will result in a jet should be lower than reality.

The water acceleration can be integrated from the water initial position ($H(t = 0)$) to any distance above the tube exit to find the velocity at that distance.

$$\int_0^z a_z \, dz = u_z(z) = \frac{2\sigma}{\rho R}\left[ln\left(\frac{H-z}{H}\right)\right] + g(H-z) \tag{4.3}$$

We are interested in finding the maximum initial fill height for a given tube radius that will result in the water stopping prior to fully exiting. Above this height, all the water in the tube will exit and external film behavior will be observed. Setting the water velocity to zero and solving for maximum initial height, H_{max} gives the solution

$$H_{max} = -\frac{2\lambda_c^2}{R}\ W\left(\frac{-f_h\, R}{2\lambda_c^2} exp\left(-f_h\, R/2\lambda_c^2\right)\right) -\ f_h \tag{4.4}$$

where λ_c is the fluid capillary length, defined as

$$\lambda_c = \sqrt{\frac{\sigma}{\rho g}}. \tag{4.5}$$

Some minimum value that must remain in the tube is chosen, as Equation 4.3 is undefined at zero height. The final height $f_h = R(1 - sin(\theta))$ is chosen, as it would be the height required to support the semicircular water bulge out of the tube after the water has settled.

4.2 Water Column Velocity Development

In cases where the modified Bond number is below unity and gravity dominates over initial capillary forces, the water accelerates down and out of the tube. Viscous forces and shear stresses cause this acceleration to be slowed at the walls (Figure 4.2b). This results in a developing velocity profile. The exact profile as it develops over time, starting from rest, has been derived by Szymanski(4), who reduced the Navier-Stokes equations with a

constantly applied pressure differential and negligible gravity of an incompressible fluid to

$$\frac{\partial u_z}{\partial t} = g - \nu \left[\frac{\partial}{\partial r} \left(r \frac{\partial u_z}{\partial r} \right) \right] \qquad 0 \leq r \leq R\,, \quad 0 \leq t, \tag{4.6}$$

with the coordinate system seen in Figure 4.1a, where u is the velocity of the fluid, t is time, z is the direction normal to the tube (i.e., down the tube), r is the radial direction from the tube center, g is the acceleration due to gravity, and ν is the kinematic viscosity of the fluid (Szymanski's original equation considers a pipe accelerated by a constant pressure differential instead of gravity. Because both the pressure differential and gravity are constant, it is appropriate to substitute the gravity term into the equation.)

The appropriate boundary conditions are the no-slip condition at the liquid-wall interface (Equation 4.7a) and a symmetry assumption in the center of the tube (Equation 4.7b). The initial condition assumes that the water column starts at rest (Equation 4.7c).

$$u_z(R, t) = 0 \tag{4.7a}$$

$$\frac{\partial u_z}{\partial r}(0, t) = 0 \tag{4.7b}$$

$$u_z(r, 0) = 0 \tag{4.7c}$$

Applying these conditions one arrives at the solution, which is an infinite series of Bessel functions

$$u_z(r, t) = \frac{g}{\nu} \left[\frac{R^2 - r^2}{4} + \sum_{n=1}^{\infty} \left(\frac{2R^2}{J_1(z_n)\, z_n^3}\, exp\left(\frac{-\nu\, z_n^2\, t}{R^2} \right)\, J_0\left(\frac{z_n\, r}{R} \right) \right) \right], \tag{4.8}$$

where, J_0 and J_1 are Bessel functions of the first kind of order zero and one, respectively. z_n is the nth zero of the Bessel function of the first kind of order zero.

4.2.1 Air Pressure Inside the Tube

As the water descends down the tube, the space it leaves behind is filled in with air from the open top. This moving air inside the tube has a lower pressure than ambient air, which can be expressed by Bernoulli's equation

$$P_1 + \frac{1}{2}V_1^2 + \rho g H_1 = P_2 + \frac{1}{2}V_2^2 + \rho g H_2, \tag{4.9}$$

where P is the pressure of the fluid, V is velocity of the fluid (which can be approximated as the velocity at the center of the water column), H is relative fluid height, subscript atm is ambient conditions, and subscript in is conditions inside the tube. In this particular case, height differences are negligible and ambient air has no velocity, so the equation reduces to

$$P_2 = P_1 - \frac{1}{2}V_2^2 \tag{4.10}$$

Pressure was found not to have a significant effect on the problem. While the water column is in the tube, the low pressure in the tube was found not to have enough force to significantly affect the water velocity. When the water column has drained and the external film has pinched off, the air is no longer moving and so the pressures would be equal to atmospheric pressure inside the tube. It is mentioned here only to inform that pressure was considered and taken into account during this study.

4.3 Film Development

The decreased velocity of the falling water near the tube wall leads to thin films being left behind the main water column. These thin films are not static, but drain down the tube far slower than the main water column. Draining films from a vertical surface fall into two main categories in this study. They are the simpler flat plate drainage and the more complicated curved surface drainage. van Rossum(13) showed that curvature on an entrained surface has negligible influence in film draining when the Goucher number $Go = R\sqrt{\rho g/2\sigma}$ (Goucher(14)) is above $\sqrt{2.5}$. Most of the tubes in this study have Goucher numbers above $\sqrt{2.5}$, so flat plate assumptions are appropriate for most of this study.

For these large Goucher number cases, computation can be done using the Cartesian coordinates defined in Figure 4.1b, which are simpler to work with than cylindrical coordinates when performing differential manipulation. The developing velocity profile of a film of given thickness starting from rest can be derived using the reduced Navier Stokes equations

$$\frac{\partial u_z}{\partial t} = g - \nu\left(\frac{\partial^2 u_z}{\partial x^2}\right) \qquad 0 \le x \le h\,, \quad 0 \le t. \tag{4.11}$$

Appropriate boundary conditions are shown in Equation 4.12a and Equation 4.12b. The no-slip condition is the same as that of the water column (Equation 4.7a), though the symmetry plane assumption used in the water column velocity profile equations (Equation 4.7b) is replaced by a zero-stress assumption at the water-air interface (h). The initial condition is the same as that used in the water column profile (Equation 4.7c), shown in

Cartesian coordinates in Equation 4.12c.

$$u_z(0,t) = 0 \tag{4.12a}$$

$$\frac{\partial u_z}{\partial x}(h,t) = 0 \tag{4.12b}$$

$$u_z(x,0) = 0 \tag{4.12c}$$

From these conditions, the expression can be expanded to

$$u_z(x,t) = \frac{g}{\nu}\left[\frac{x^2}{2} - xh + 2h^2\sum_{n=1}^{\infty}\left(\frac{1}{\alpha_n^3}exp\left(\frac{-\alpha_n^2\nu t}{h^2}\right)sin\frac{\alpha_n x}{h}\right)\right], \tag{4.13}$$

where α_n is $\pi(n-1/2)$. This was originally derived by Green(16) and Wyllie(17). Integrating over the film thickness to obtain the flow rate per transverse length, q yields,

$$q(x,t) = \frac{1}{h}\int_0^h u_z\, dx = \frac{gh^3}{3\nu}\left[1 - \sum_{n=1}^{\infty}\left(\frac{6}{\alpha_n^4}exp\left(\frac{-\alpha_n^2\nu t}{h^2}\right)\right)\right]. \tag{4.14}$$

Multiplying (Equation 4.14) by h and substituting into continuity (Equation 4.15) reveals the film profile Equation 4.16 which is plotted in Figure 4.3. This derivation comes from Annapurna and Ramanaiah(18), who provided a derivation that corrected errors in an earlier attempt by Gutfinger and Tallmadge(12).

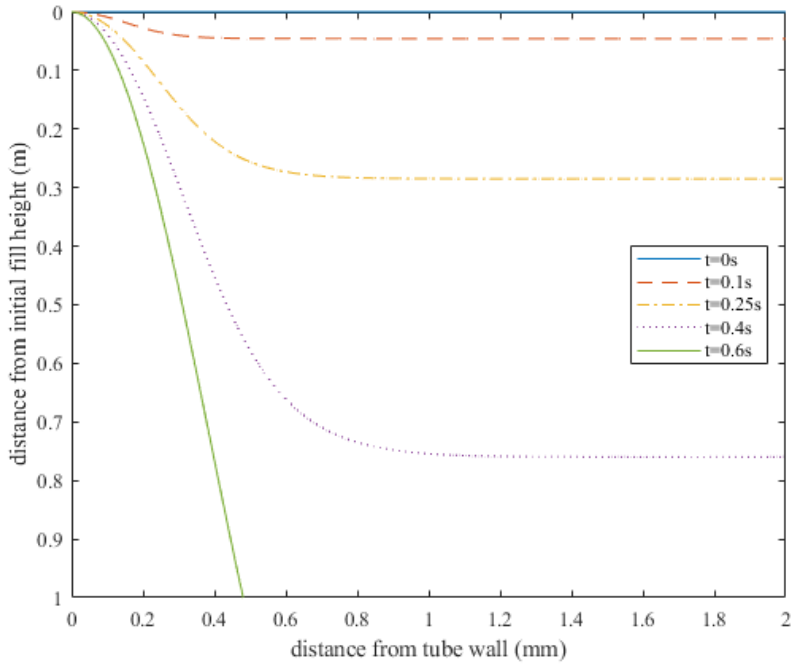

Fig. 4.3: Film profile development over time. As the main body of water exits the tube, the remaining film continues to thin and flow.

$$-\frac{\partial h}{\partial t} = \frac{\partial}{\partial z}\left(\int_0^h u_z \, dx\right), \tag{4.15}$$

$$z(h,t) = \frac{g}{\nu}\left[h^2 t - \frac{2h^4}{3\nu} + \frac{2h^4}{\nu}\sum_{n=1}^{\infty}\left(\frac{1}{\alpha_n^2} exp\left(\frac{-\alpha_n^2 \nu t}{h^2}\right)\left(5 + \frac{2\alpha_n^2 \nu t}{h^2}\right)\right)\right], \tag{4.16}$$

This film profile development is used to find the exit conditions of the film over time for a given initial fill height. Figure 4.4 shows typical film exit over time with three different initial fill heights. As fill height increases, so does time until film emergence, initial film thickness, and initial exit velocity. In all cases, film thickness and velocity have an initial steep decline, followed by an asymptotic approach to zero. Near steady-state film thickness

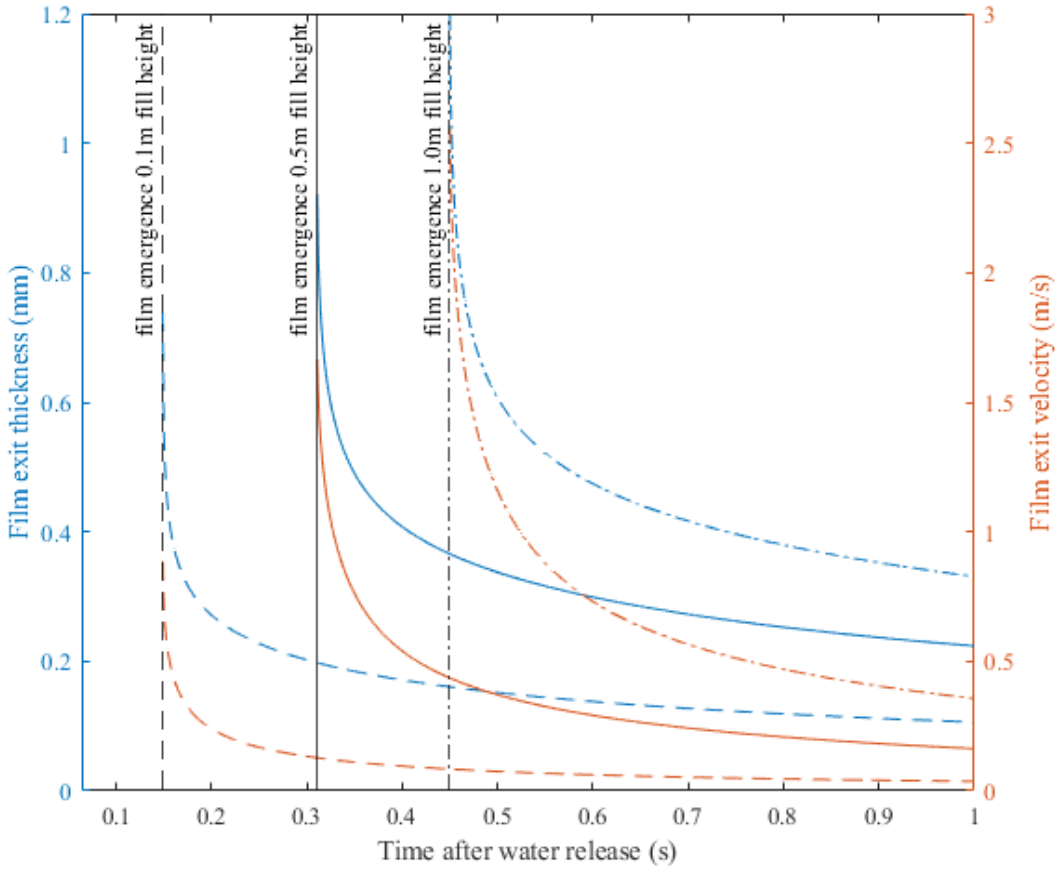

Fig. 4.4: Typical film exit thicknesses and velocities over time, given that Goucher number is at least $\sqrt{2.5}$. Film exit thickness and velocity initially undergo a relatively steep decline, followed by an asymptotic approach to zero. As the initial fill height of the water increases, the initial exit thickness and velocity increases while the asymptotic decline becomes less extreme.

and velocity are reached sooner in lower fill height cases, with higher negative slopes in higher fill height cases.

When the Goucher number is below $\sqrt{2.5}$, the curvature of the tube is no longer insignificant in film development, and the equations used must be modified somewhat. The transient velocity profile of a curved film starting from rest cannot be solved outright using the Navier-Stokes equations, as was done when finding the transient water column and flat

film velocity profiles. However, flat plate assumptions continue to work reasonably well when the film is small relative to the tube radius, represented by the variable $\eta = h/R$ (Gutfinger and Tallmadge(12)).

In order to find the maximum value of η where flat plate drainage can represent curved surface drainage, the inertial steady-state values of thickness and velocity are compared between curved and flat plates. A film that has reached inertial steady-state has balanced viscosity and gravity to reach a fully developed velocity profile as a function of thickness. Inertial steady-state films are not true steady state films, as the velocity profile is a function of film thickness, which in a draining film is continually decreasing with time. If the inertially steady-state film thicknesses and velocities are sufficiently similar between the flat and curved films, then it can be reasonably assumed that the transient solutions are also fairly similar. Gutfinger and Tallmadge(12) compared the flat and curved draining film thickness solutions. The draining film profile on a flat plate, derived by Jeffreys(11) is found using the reduced Navier-Stokes equation seen in Equation 4.11 with the time derivative set to zero and coordinate system of Figure 4.1b. The boundary conditions Equation 4.12a Equation 4.12b are applied to find the velocity profile

$$u_z(x) = \frac{g}{\nu}(hx - \frac{h^2}{2}) \tag{4.17}$$

which is integrated over the film thickness and divided by the thickness to find the average film velocity

$$\bar{u}_z = \frac{gh^2}{3\nu} \tag{4.18}$$

Equation 4.17 is substituted into continuity (Equation 4.15) to find the film thickness equation, given in terms of depth as a function of thickness and time

$$z(h,t) = h^2 \frac{gt}{\nu}. \tag{4.19}$$

The equivalent curved solution is found using the reduced Navier-Stokes equations are in Equation 4.11 with the time derivative set to zero and r defined from the tube radius minus the film thickness, $R-h$, to the tube radius R, using the coordinate system of 4.1a. The boundary conditions are the same as Equation 4.7a Equation 4.7b, with the exception that Equation 4.7b is equal to zero at the r value $R-h$. The velocity profile is then

$$u_{z\,curved}(r) = \frac{g}{2\nu}\left[\frac{R^2-r^2}{2} + (R-h)^2 ln\left(\frac{r}{R}\right)\right] \tag{4.20}$$

This is integrated across the thickness and around the diameter, then divided by the area to find the average velocity

$$\bar{u}_{z\,curved} = \frac{g}{2\nu(R^2-(R-h)^2)}\left[\frac{R^4}{4} - R^2(R-h)^2 + (R-h)^4\left(ln\left(\frac{R}{R-h}\right)\right)\right] \tag{4.21}$$

which is substituted into continuity

$$-\frac{\partial q}{\partial z} = 2\pi R \frac{\partial R}{\partial t} \tag{4.22}$$

(where q is the flow rate per circumference length), to find the film profile expressed with the depth as a function of the film height and time

$$z(h,t) = \frac{gt}{\nu}\left[h\left(R - \frac{h}{2}\right) + (R-h)^2 ln\left(1 - \frac{h}{R}\right)\right] \tag{4.23}$$

Nondimensional film thickness, H, can be defined as the curved film thickness divided by the flat film ratio in Equation 4.19

$$H = h\sqrt{\frac{gt}{\nu z}} \tag{4.24}$$

By nondimensionalizing Equation 4.23 using H and η, it can be shown that steady-state film profiles differ according to the dimensionless relationship

$$H^2 = \frac{\eta^2}{(1-\eta)^2\, ln(1-\eta) + \eta(1-\eta/2} \tag{4.25}$$

A similar relationship is derived here to find the difference between the flat and curved film velocities. Non-dimensional film velocity, V, is defined as the curved film velocity divided by the equivalent flat film velocity in Equation 4.18

$$V = \frac{gt^2}{3\nu} \tag{4.26}$$

Equation 4.21 can then be rewritten in non-dimensional terms V and η

$$V = \frac{3}{2\eta^2\,(1-(1-\eta)^2)}\left[\frac{1}{4} - (1-\eta)^2 + (1-\eta)^4 ln\left(\frac{1}{1-\eta}\right)\right] \tag{4.27}$$

Using these relationships, the percent difference between a curved film and flat plate film and curved film relative to η is shown in Figure 4.5.

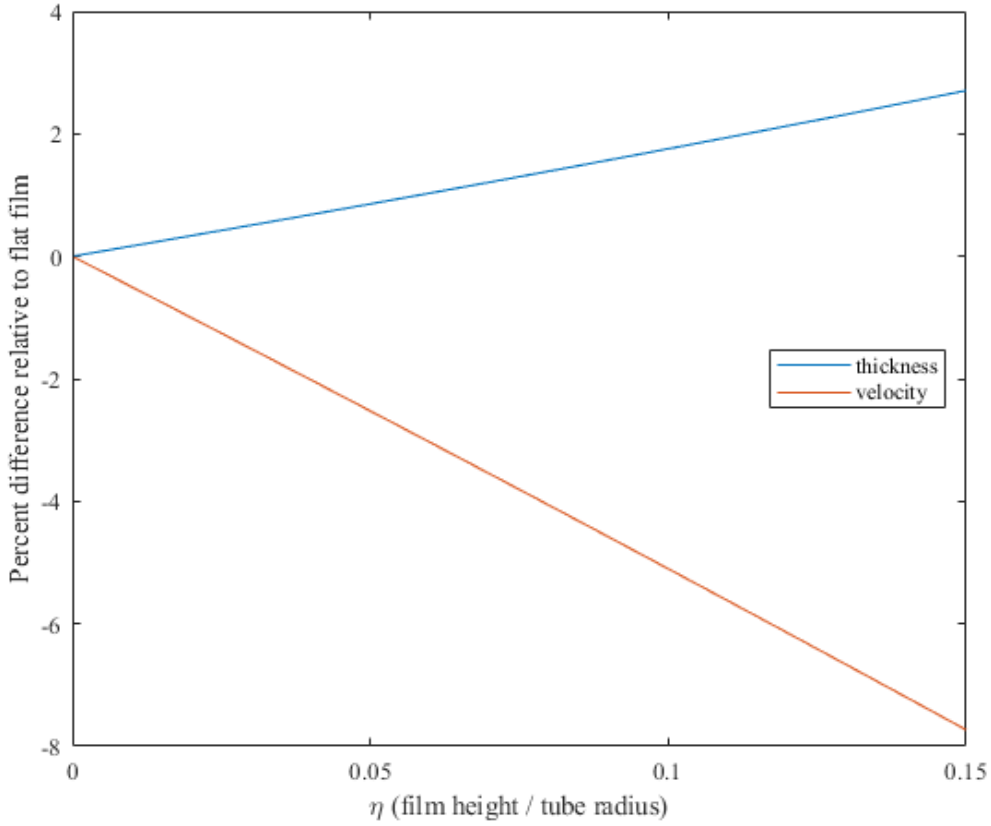

Fig. 4.5: Thickness and velocity ratios for films on flat vs. curved surfaces, showing the percent that curved films deviate from flat films.

This shows that tubular films are both thicker and slower than equivalent films on flat plates. Based on figure 4.5, it can be seen that using flat film equations are reasonable for η values of up to 0.06 for velocity, and up to 0.11 for thickness, when steady-state values differ by only 2% from the curved case. Above these thicknesses, the velocity and top film profiles created by the accelerating water column are used.

4.4 Film Waves

As films travel down solid surfaces, they soon develop waves due to surface tension amplification of small disturbances in the wave surface. The waves are initially highly irregular, but over time develop a somewhat more consistent frequency and size. The extensive empirical data on the development of water films over time collected by Takahama and Kato(30) and Takamasa and Kobayashi(31) has been digitized to find empirical models to predict the film's maximum and minimum heights, as well as the dominant wave frequency and wave speeds vs. time, as shown in Figure 4.1c. The maximum film height (i.e. film thickness at the wave peak) can be expressed as,

$$h_{max} = h_{mean} \frac{Re^{0.2924} L^{0.6054} \rho}{Ka^{.0514}} \tag{4.28}$$

where Re is the film Reynolds number, which shows the relative magnitude of inertia to viscosity, defined as,

$$Re = \frac{\bar{u}_z h}{\nu}. \tag{4.29}$$

Here, L is the distance that the film has travelled, and $Ka = \sigma/(\rho\nu^{4/3} g^{1/3})$ is the Kapitza number, a dimensionless term that shows the relative magnitude of surface tension to viscous

and gravity forces.

The minimum film thickness (thickness at the trough of the wave) has been found to eventually stabilize, regardless of initial film thickness and is defined as,

$$h_{min} = 6e - 4L^{-6.8333} + 4.54\left(\frac{g}{\nu^2}\right)^{-1/3}. \tag{4.30}$$

The last term in Equation 4.30 is the minimum film thickness equation, which is the predicted eventual steady-state trough height of wavy films (Ito and Sasaki(29).

Wave frequency also plays an important role in the observed behavior. As the waves in the film descend down the tube, they often merge together, increasing the distance between waves. This transient behavior causes the wave frequency to steadily decreases until it reaches a stable frequency. The stable frequency for water is approximately 10Hz (30). The dominant frequency of the waves based on distance the film has travelled has also been empirically modelled as

$$f = 12.66\, e^{-.0628*L} + 4881\, e^{-13.23*L}, \tag{4.31}$$

which approaches 10Hz after about 700mm.

Using all of these empirical predictions of wave development, a reasonable approximation of the wave development can be estimated and incorporated into the previous film drainage model (equation 4.27) to find the film thickness at tube exit vs. time. A typical example of this wave development can be seen in Figure 4.4, using a 0.5mm film. The wave frequency is seen to decline fairly steadily and then level out to the steady-state frequency of 10Hz. The minimum wave height also initially decreases and then approaches the steady-

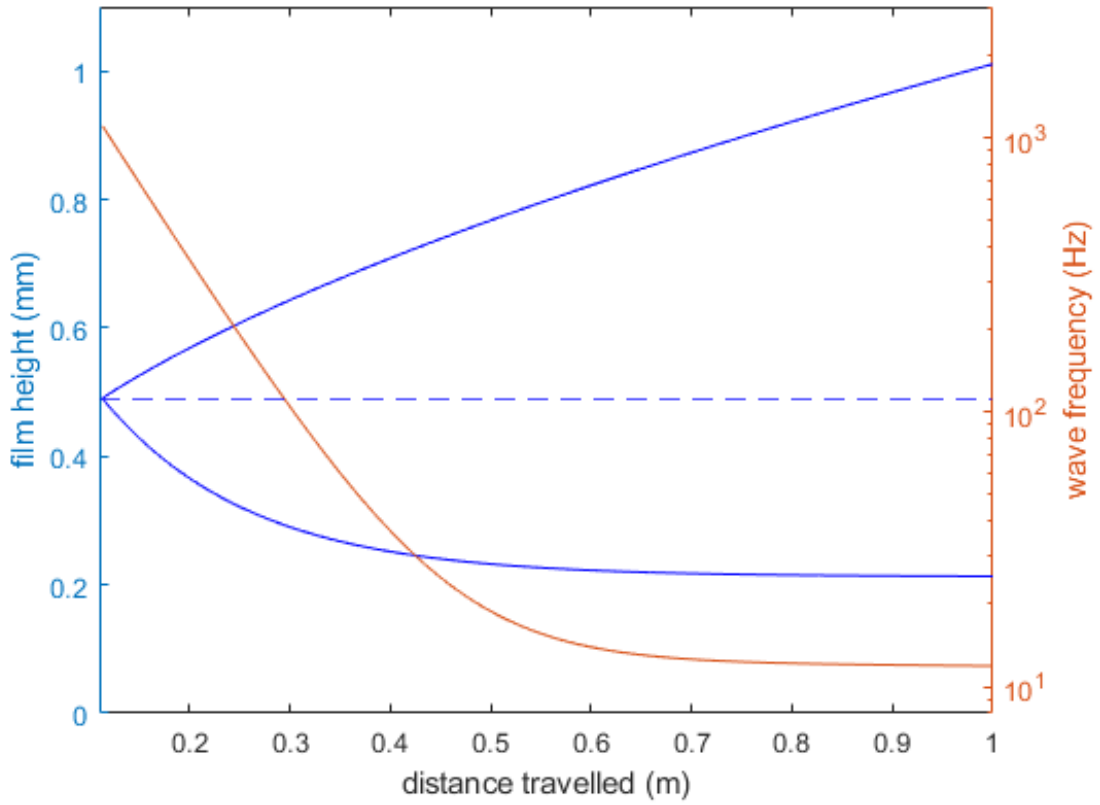

Fig. 4.6: Film expected maximum and minimum film heights over time, as well as typical frequency over time. The starting film height is 0.5mm.

state trough height. The maximum film thickness increases at a decreasing rate throughout the distance travelled.

4.5 Water Bells

When the film initially exits the tube, it is a tubular shape with the film outer radius equal to the inner radius of the tube. The shape of the falling film is then governed by gravity, pressure differences between the air inside and outside of the film, surface tension, and inertia (Figure 4.2c), which interact to form vertically projected water bells, or fluted films. The balance of these forces normal to the film has been expressed by Boussinesq(36;

37), shown in Equation 4.32, with the coordinate system shown in Figure 4.1d.

$$\frac{2\sigma}{r_c} + \frac{2\sigma cos(\psi)}{r} - sin(\psi)g\rho T = \frac{\rho T u_{z'}^2}{r_c} \tag{4.32}$$

where r is the radial distance of the outside of the film from the tube center, z' is the vertical (downward) distance of the film from the tube exit, ψ is the angle from vertical of the film (where a positive ψ is angled inwards, towards the radial center). The initial ψ value at the tube exit is equal to $\theta' - \pi/2$, where θ' is the dynamic wetting angle of the tube. T is the thickness of the film, r_c is the radius of curvature of the film, $u_{z'}$ is the velocity of the film in the z' direction, and the subscript 0 represents conditions at tube exit. The surface tension effects referred to here come from liquid surface curvature, as seen in the Young-Laplace equation,

$$\Delta P = \sigma \left(\frac{1}{r_1} + \frac{1}{r_2} \right) \tag{4.33}$$

where r_1 and r_2 are the radii of curvature. This effect only acts normal to a surface, and so does not have a tangential affect on the film. Gravity alone acts tangentially on the film, expressed as a change in film velocity in

$$u_{z'} = \sqrt{u_{z'0}^2 + 2gz} \tag{4.34}$$

The flow rate of the film, Q, is found using continuity in

$$Q = \pi u_{z'} \left(2rT - T^2 \right) \tag{4.35}$$

The flow rate remains constant as the film travels downward, and is found using the initial (tube exit) film thickness, radius, and velocity. It is worth noting that this flow rate function is slightly different than those used in most other water bell calculations. The water bells seen in Lance and Perry(43), and in water bell research in general, tend not to pinch off, but instead terminate by disintegration or impingement onto either a solid surface or quiescent water. Because of this, the film thickness is always small relative to the radius, so the thickness squared term can be taken as negligible. The water bells examined in this project pinch off when the film contacts itself, which occurs when the radial film thickness is equal to the film radius. Therefore, the thickness squared terms is not always negligible, and is added to the equation. The thickness of the film, T, is found by rearranging the continuity equation,

$$T = r - \sqrt{r^2 - \frac{Q}{\pi u_{z'}}} \tag{4.36}$$

4.5.1 Numerical Solution to the Water Bell Equation

Equation 4.32 cannot be solved outright. Instead, the numerical method of Lance and Perry(43) can be employed to find the film shape and pinch-off point, where pinch-off point is defined as the vertical distance between the tube exit to the point where the film pinches into a water stream.

Careful examination of the inertial and surface tension forces in equation Equation 4.32 reveal that the water bell equation cannot be solved if the Weber number is below two. This critical Weber number will be discussed more in Section 4.5.2.

The water bell shape can be numerically found by first using the exit conditions of the film (i.e. at $z' = 0$) to find the radius of curvature and center of curvature of the film at

that point. These are used to calculate the position and thickness of the film at some small distance just below the tube exit, $\Delta z'$. The shape properties of the film are then calculated at this point to find the film thickness and radius at $\Delta z'$ below this point, and so forth until the entire water bell shape is found. The end of the water bell is the pinch-off point, where the thickness of the water film equals the film radius.

The numerical driving factor used here is distance from the tube opening. For example, a film at numerical step i is at distance $z'(i)$ from the tube opening. At step $i+1$, the film is at distance $z'(i+1) = z'(i) + \Delta z'$ from the tube opening. The distance $\Delta z'$ is any arbitrary small value, with the value used in this study being $1 * 10^{-4} m$, or one tenth of a millimeter. At the tube opening, $z'(i) = 0$ and the film outer radius is equal to the tube inner radius. The film thickness and velocity at the tube opening are the exit film thickness and velocity discussed in 4.13. The initial film angle relative to vertical, psi, is assumed to be $\theta_d - \pi/2$, where θ_d is the dynamic wetting angle of the tube defined by Terpilowski et al.(55).

Consider a film at some numerical step i. In order to calculate the film at the next numerical step, the radius of curvature, $r_c(i)$, of the film at must first be found. This is found by rearranging equation 4.32 to

$$r_c(i) = \frac{\rho T(i) \ \left[U_{z'}(i)^2 + 2gz'(i)\right] - 2\sigma}{2\sigma cos(\psi(i))/r - gT(i) \ sin(\psi(i))}. \tag{4.37}$$

The location of the center of curvature (radial and vertical coordinates being $c_r(i)$ and $c_z(i)$, respectively) is then defined as

$$c_r(i) = r(i) - r_c(i) \ cos(\psi(i)) \tag{4.38}$$

and

$$c_z(i) = z'(i) - r_c(i)\ sin(\psi(i)). \tag{4.39}$$

The film will follow this curvature for a small distance, $\Delta z'$. The radius of the film at this new distance, $z'(i+1) = z'(i) + \Delta z'$ is found using the radius and center of curvature at i, written as

$$r(i+1) = c_r(i) - \sqrt{r_c(i)^2 - (z'(i+1) - c_z(i))^2}. \tag{4.40}$$

The new angle of the film relative to vertical, $\psi(i+1)$ must now be found at this new point. To do this, the total distance between the film at i and $i+1$, $d(i+1)$ is found using the Pythagorean theorem, shown as

$$d(i+1) = \sqrt{\Delta z'^2 + (r(i) - r(i+1)^2)}. \tag{4.41}$$

The angle of rotation between the film at i and $i+1$, $\phi(i+1)$ is

$$\phi(i+1) = 2asin\left(\frac{d(i+1)}{2r_c(i)}\right) \tag{4.42}$$

which is added to $\psi(i)$. The water film velocity, $U_{z'}(i+1)$, can now be calculated as

$$U_{z'}(i+1) = \sqrt{U_{z'}^2(i) + 2g\Delta z'} \tag{4.43}$$

and the new film thickness is

$$T(i+1) = r(i+1) - \sqrt{r(i+1) - \frac{q}{\pi U(i+1)}}. \tag{4.44}$$

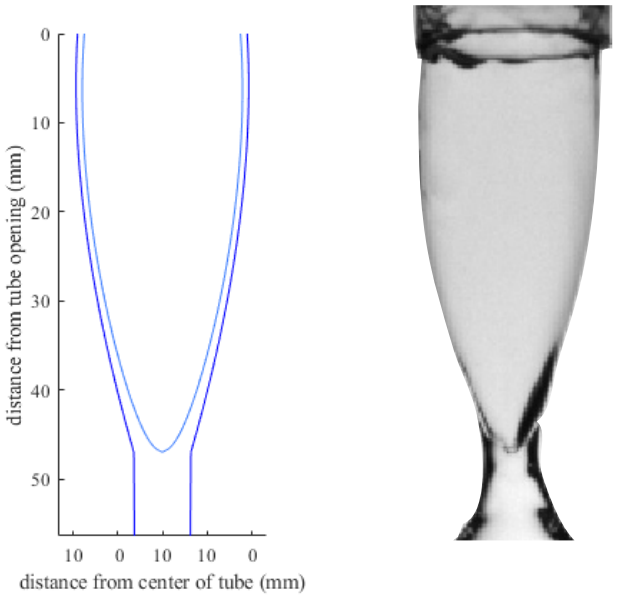

Fig. 4.7: Typical calculated vs. actual fluted film shape. This fluted film was calculated using a tube of radius 9.5mm filled with water to a height of 7.62cm.

The process can then be repeated until pinch-off is reached.

The shape of a typical water bell and subsequent water jet can be seen in Figure 4.7. The comparison here is a particularly good one. For a more detailed comparison of the modelled vs. observed shapes, see Section 5.5.

It is observed in the experiment phase of this study that when the film pinch-off point is less than one radius of tube, the film will quickly retract into the tube and form a horizontal film across the tube bottom (see Figure 3.1d). This is likely due to adhesion between the water and the tube exit, since the tube is hydrophilic.

4.5.2 Falling Film Breakup

The falling water films are not always stable, sometimes breaking up into small droplets. This instability arises from the interaction of surface tension and inertial forces (Taylor(45)).

The pull of surface tension acts to decrease surface area (and therefore decrease the energy state) of a liquid surface. Because thin liquid films have a very large surface area, they are in a high surface energy state, and surface tension attempts to pull the film into small droplets, decreasing the surface energy. This force is counteracted by the film's inertia, which is the tendency of matter to resist change in velocity. As long as inertia is greater than surface tension, the film is unable to break up into droplets and will remain unbroken. The ratio between inertial and surface tension forces on a surface is commonly given by the Weber number

$$We = \frac{\rho u^2 L}{\sigma} \tag{4.45}$$

where u is the characteristic velocity and L is the characteristic length. In this case, the characteristic velocity is the film velocity and the characteristic length is the film thickness. Because the film is double sided, the effects of surface tension are doubled, so a Weber number above two would coincide with inertial forces dominating surface tension, not allowing the film to break (Taylor(45)). If the Weber number is below two, surface tension will dominate and the film will break up (as seen in Figures 3.1f-j).

4.6 Predicting External Film Behavior

The wide variety of external film behaviors seen in the experiments can be predicted by comparing the Weber numbers and pinchoff points of the film over time. As was mentioned earlier, the Weber number determines whether or not the film will disintegrate, with the critical breaking value being two for a two-sided film. By calculating the exiting film Weber number over time using the film equations in 4.3 and 4.4, it can be determined when the film will break up.

4.6.1 Film Breakup Before Pinch Off

If the film breaks up at the tube exit prior to pinchoff, the film forms the *Crown and bell* in Figure 3.1h. This can be seen in Figure 4.8a, where the Weber number descends below the critical breaking value before the initial film pinch-off. It is important to note that the critical value used to determine whether or not the film will break prior to pinch-off is one, instead of the value of two discussed earlier. This is because the film breakup prior to initial pinch-off always occurs right at the tube exit. Prior to exit, the film that is entrained on the tube wall has a critical Weber number of one, as it only has one surface exposed to the air. If the film has a Weber number below one, it is unstable prior to exiting the tube, and should begin to break up before or immediately upon exit. On the other hand, a film with a Weber number between one and two only becomes unstable after exit, and this instability may take some time to break up the film. Further, using a critical Weber number of one when determining whether or not the film will rupture prior to pinch-off compares favorably with experimental results.

4.6.2 Retraction vs. Breakup

If the film does not rupture prior to pinch-off, one of several other behaviors is possible. It was observed that films that when film pinch-off is closer than one tube radius, it quickly retracts into a horizontal film across the tube exit. A pinch-off point of one tube radius or less can therefore be considered the critical pinch-off point, when the film will cease to be a water bell without breakup. By comparing when the Weber number and pinch-off points cross their critical values, it can be determined whether or not the film will break. The critical Weber number used in this instance is also different than the critical value of

two reported by Taylor. This is a result of the intense forces that the water bell undergoes when retracted into the tube. When retracted, the film does not immediately settle into a horizontal film, but is pulled into the tube with such force that it oscillates several times up and down before settling in a horizontal position. This intense film stretching results in film breakup when the Weber number is near two. However, the film tends to fare better if it is at a Weber number of four or higher. Therefore, a critical Weber number value of four is used in this segment. If the Weber number falls below its critical value before the pinchoff point crosses its critical value of one tube radius (Figure 4.8b), the water bell will break, as in the *Breaking champagne* behavior seen in Figure 3.1f. If the pinchoff point crosses the critical point before the Weber number (figure 4.8c), the water bell will retract into the tube as seen in the *Retracting champagne* behavior of Figure 3.1d.

4.6.3 Multiple Pinch-off

Sometimes the film will not pinch off at the film-water column interface, but will pinch somewhere father up the film. This occurs when the film initially exiting the tube has a longer pinchoff time than the film that emerges later. This film behavior is called *Symmetric champagne* and can be seen in Figure 3.1i. This can be seen theoretically in Figure 4.8b, when a single pinch point diverges into two lines, travelling both upward and downward simultaneously over time. This can be understood as the "stem" of the champagne glass getting longer as it expands both up and down at the same time.

The existence of a diverging pinch-off point does not necessarily guarantee the *Symmetric champagne* behavior, however. Occasionally, the initial pinch-off point will occur so close to the film-water column interface that no secondary pinch off can occur. Instead, only

a tiny bubble is captured between the water column and initial pinch-off. The bubble tends to be roughly the same diameter as the post pinch-off jet. Although air is trapped below the initial pinch-off, this is not considered a true multiple pinch-off event, as the bubble is small and stable enough to prevent a secondary pinch-off point from travelling in the direction of the water column. This would be seen theoretically by an initial pinch-off point diverging, followed by one of the diverged branches ceasing almost immediately afterwards. Therefore, only pinch-off point charts that have significant secondary pinch-off points (i.e. lasting longer than one millisecond) are predicted to result in the *Symmetric champagne* behavior.

4.6.4 Waviness Effects

Similar to the derivation of the waviness equations, the effect that waviness has on the film behavior is largely empirical. By careful comparison of the calculated wave conditions of the film to waviness effects seen in the experiment, threshold values for different behaviors can be found.

Three wavy behaviors have been observed. They are *Multiple slug*, *Jumping champagne*, and *Bubble* (Figure 3.1c, e, g, respectively). In all cases, the oscillating waves that develop on the film result in some sort of periodic behavior occurring outside of the tube. In the case of the *Multiple slug* behavior (Figure 3.1c), the waves have reached a large enough height to connect across the tube, and become a series of water slugs separated by air pockets. In the *Jumping champagne* case (Figure 3.1e), the film pinches off in an elongated Champagne shape, with the pinch point periodically 'jumping' closer to the tube exit until it secedes into the tube. In the *Bubble* behavior (Figure 3.1g), the film experiences pinch-off in multiple

places simultaneously, forming bubbles.

It is clear from the experiments performed in this study that waviness effects are only seen when the fill height of the water is relatively high. This is because the waves begin as imperceptible disturbances that increase in size as they travel down the tube. A higher fill height corresponds to a longer distance for the film to travel before exiting, and so larger and more developed waves. It is only when the eaves have reached a critical size that wave effects are visible. Tube radius and absolute wave peak height were determined not to play a significant role in the presence of waviness. Instead, a ratio of film peak height to film average height of 1.5 was determined to be the threshold for observable waviness effects.

When the wave height in a tubular film exceeds a critical point, the peaks of the wave will adhere to each other and close off, forming a water slug (Ogrosky et al.(25), Camassa et al.(24)). Eventually, the tube will be full of a long series of water slugs, separated by a distance approximately equal to the wavelength. The critical value for this behavior was found to be film maximum height equalling half the tube radius. The external behavior seen as a result is the *Multiple slug* behavior (Figure 3.1c), with slugs repeatedly creating, inflating, and destroying bubbles attached to the tube exit.

If the film waves do not contact each other in the tube, the *Multiple slug* behavior is not seen. Instead, the wavy film will exit the tube and influence the pinch-off location and time of the fluted film. Waviness can have a significant effect on film pinch-off. This is because film pinch-off is dependent on film thickness, and wavy films have a varying thickness in time. Thicker films pinch off farther from the tube and later in time than thinner films, due to their greater mass and inertia. The peak of a film wave will therefore have a farther pinch point than a relatively thin wave trough. This results in pinch-off occurring simultaneously

in multiple locations at a given time, which forms bubbles, seen in Figure 3.1g.

However, bubbles are not guaranteed in all instances. If the wave peaks and troughs are too close together (i.e. have too high a frequency), they will be prevented from separating into their respective pinch-points by surface tension cohesion. They will instead have a single pinch-off point somewhere between the theoretical peak and trough pinch-offs. A small tube radius would also restrict bubble formation, for two reasons. First, small-radii tubes create relatively short water bells, so peak and trough pinch points would be closer together than films in large tubes. This would make them more subject to surface tension cohesion, favoring a single pinch-off. Second, small tube films have much smaller cross-sectional areas than large tube films. This decreases total mass and inertia, which permits the film to move more easily, allowing it to quickly 'zip' together to a new pinch-off point when needed. These factors together lead to a film that does not form bubbles, but instead has a single pinch-off point that quickly jumps to new higher locations. This is called the *Jumping champagne* behavior, and can be seen in Figure 3.1e. To predict when this behavior will occur instead of the *Bubble* behavior, the expected distance between waves needs to be calculated. Using the calculated average film velocity and dominant wave frequency over time, the approximate expected distance between waves can be found. Multiplying the wavelength and tube radius together and then dividing by the capillary length squared gives a nondimensional factor. By observation, it is found that when this factor is below 50, the *Jumping champagne* behavior is observed, while values over 50 result in the *Bubble* behavior. This value is based on the values for the nine observed *Bubble* cases and two *Jumping champagne* behavior, which is a fairly small sample size, so further refinement in future experiments may be called for.

4.6.5 Tubular Film

The reason for the existence of the *Tube* behavior (Figure 3.1) is not immediately clear at first glance. There seem to be no distinguishing features in the wave properties or Weber/pinchoff charts that would clearly distinguish the tube behavior from the others. The answer may lie with Taylor(44), who noted that air drag can have a noticeable effect on water bells, with velocity losses up to several percent when the water bell is large. While most of the water bells have lengths of only a few centimeters between the tube exit and pinch-off point, the combination of large tube diameter, high film velocity, and large film thickness in the two *Tube* cases have estimated initial pinchoff lengths in excess of 40cm. The air drag on these long, fast moving films may slow the film and disturb the surface enough to cause rupture. The Reynolds numbers of the air around of both tube cases (with the characteristic length being the water bell length and the velocity being the velocity of the water bell film) are 88,606 and 106,216, whereas the maximum Reynolds number around the surrounding cases were all less than 60,000. This gives strong evidence that shear drag is playing a role. Therefore, the critical line between the bubble and tube cases is set at roughly halfway between, at $Re = 75,000$.

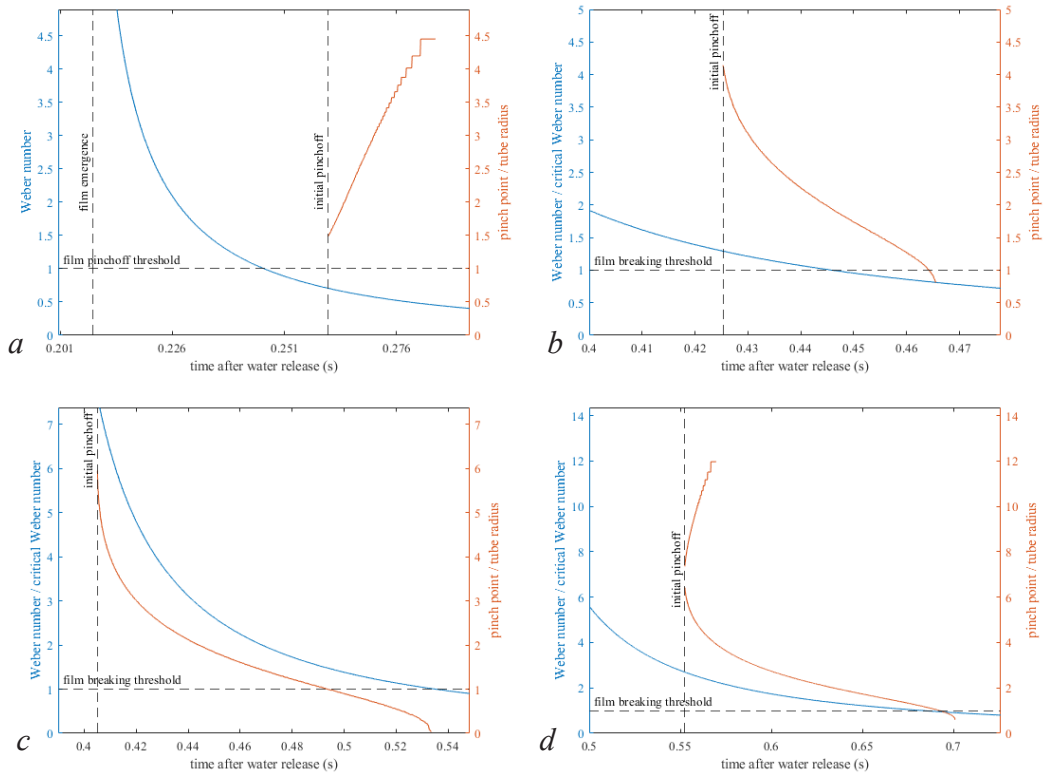

Fig. 4.8: Weber number and pinch-off point charts. Pinch-off point is defined as the distance between the tube exit and the point at which the water film pinches into a stream. The Weber number and film pinchoff points are nondimensionalized against their critical points to predict various behaviors. (a) Film disintegration prior to film pinch-off. In this instance, the Weber number falls below one prior to the initial film pinch-off. This results in the *Crown and bell* behavior in Figure 3.1h, where the film is broken when no pinch-off has yet developed. (b) Film break up. The Weber number is above one at initial pinch-off, indicating that the film successfully pinches off, resulting in a *Champagne* shape. The Weber number descends below its critical point of four before the film pinch-off descends below the critical distance of one radius. This means that the fluted film will eventually break, described by the *Breaking champagne* behavior seen in Figure 3.1f and in Figure 1.1. (c) Film retracting into the tube. Here the film successfully pinches off into the *Champagne* shape, and the film pinch-off point descends below one radius before the Weber number crosses its critical value. This means that the film will retract back into the tube and will not rupture. This behavior is known as *Retracting champagne* and is seen in Figure 3.1d. (d) Multiple pinch-off. The film pinches off, but the pinch-off point diverges in two different directions. This indicates that there are two pinch-off points, with one travelling upwards and another travelling downwards. Between these pinch-off points, the film has already pinched off and is now a stream. This behavior, known as *Symmetric Champagne*, can be seen in Figure 3.1i, seen where there is film both above and below a pinched off stream.

CHAPTER 5

DISCUSSION OF MODEL VALIDITY

Overall, the behavior of the draining water observed in the experimental portion of this study were reflected very well by the model. Because the development of the film inside the tube is not observed, that portion of the model cannot be directly validated. However, the external film behavior is directly affected by the events inside the tube, and so their validity can be inferred by the accuracy of the external film data. The overall observed vs. predicted values are shown in Figure 5.1. An explanation of how the predicted boundary lines are derived, as well as discussion on how the different portions of the model fare, are outlined below.

5.1 Boundary Line Derivation

In order to generate the predicted boundaries between different behaviors seen in Figure 5.1, two different methods are used. The trivial behavior boundaries (*Static slug* and *Jet*) are calculated outright using equations 4.1 and 4.4, respectively. The non-trivial behavior boundaries are found using a more complex method. First, the exiting film conditions, wave variables, and pinch-off points are computed over time across a dense grid of tube sizes and initial water fill heights using the equations in 4.3,4.4, and **??**, respectively. The methods described in 4.6 are coded to predict the behavior outcome of each point on the grid (i.e. for each tube size and fill height). The boundary points between behaviors are then put into curve fitting programs to generate the lines seen in Figure 5.1.

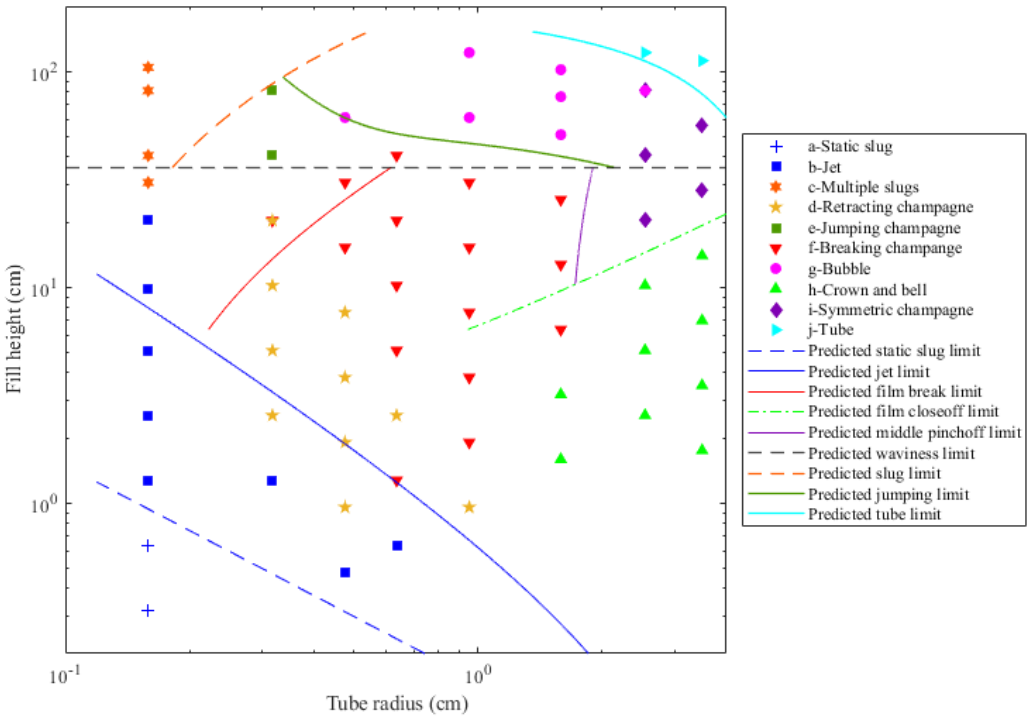

Fig. 5.1: Observed vs. Prediction behavior. The predicted boundaries between different behaviors are shown with lines, while the observed behaviors are represented with points.

5.2 Trivial Behaviors

There are two trivial behaviors, or behaviors that did not produce external films. The first behavior is that of *Static slug* (Figure 3.1a), where no water exits the tube. Equation 4.1, which can be used to predict the upper boundary of this behavior, is shown compared to observed behavior in Figure 5.1. The theoretical limit compared very well to the observed experiments, with both of the *Static slug* cases lying beneath the predicted limit.

The other trivial behavior is the *Jet*, seen in Figure 3.1b, where some water escapes the tube, but some is left behind. The upper limit of this behavior predicted by Equation 4.4 captured the overall trend quite well. As was discussed in Section 4.1.2, the assumptions for this equation include negligible viscosity effects in the tube center. This assumption begins to break down when the tube is small and the fill height is large. Because tube center velocity with significant viscosity would be slower than the model predicts, the momentum that surface tension would need to overcome to stop the flow would be lower. Therefore, in theory, the model should under-predict the maximum *Jet* height at the lowest tube sizes.

5.3 General External Film Behavior

The model distinguishing between external film behaviors, outlined in Section 4.6, overall compares quite well to observed behaviors. The predicted limit of the film closing before pinchoff, which distinguishes the *Crown and bell* behavior ((Figure 3.1h) from other external film behaviors, agreed very well with the observed behavior. The middle pinching prediction, which distinguishes the *Symmetric champagne* (Figure 3.1i) from other cases, also performed very well against the observed behavior.

The film breaking limit, which predicts the divide between *Breaking champagne* and *Retracting champagne* (Figure 3.1d and Figure 3.1f, respectively) is less accurate. This limit only partially capture the observed trends. The trend of film break occurring at higher tube sizes is captured by the model, while the trend of film break occurring at greater fill heights was not. This incorrect line slope indicates that there may be more factors that the model currently does not take into consideration. For example, a larger diameter may allow for larger oscillations when the film is retracted, which would increase the surface area and decrease the thickness of the film, making it more likely to break.

Films were observed that had a predicted Weber number of less than two. Unfortunately, the water bell equations are undefined at Weber numbers below two, and so predictions for external film behavior with an initial fill height of under about 6 cm could not be generated. Simply extending the existing calculated limit lines does not seem to fit the lower fill height data very well.

5.4 External Film Waviness Behavior

The experimental wave behaviors agree well with the empirically derived predictions. The wavy behavior threshold captures the observed wavy cases fairly well, though there seems to be a slight tube size effect that is not captured. Overall it compares well with Takahama and Kato(30), who observed that significant waves were not observed in the first 500 mm or so for films below roughly $Re = 1000$. The *Tube* and *Jumping champagne* dividing lines also reflect the experiment well.

Several of the tube phenomenon have very few observed data points, making it difficult to know with certainty what is causing the behavior. For example, the *Jumping champagne*

behavior is only seen in one experimental tube size, which makes it very difficult to discern which factors are driving the behavior. However, the models derived for these sections were made not just by looking for associations, but by considering very carefully how different factors may interact and how the physics behind the phenomena likely works. It will be interesting to compare these tentative theories and correlations to future studies with more data in this upper region.

5.5 Water Bell Shape

The water bell shapes predicted by the model reflect the experimentally observed shapes fairly well. A simple comparison of the initial pinch-off points gives a general idea of the accuracy of the modelled shapes, where pinch-off point is defined as the distance between the tube opening and the pinch off of the water bell. The ratio of modelled vs. observed initial pinch-off points is seen in Figure 5.2. The model predictions are all between 0.5 and 1.7 times the observed initial pinch-off points, with most predictions between 0.65 and 1.2. This is a surprisingly low amount of variation, considering the transient nature of the film and the many behaviors observed. The average ratio is 0.87, which is satisfactorily close to one. Possible explanations for the observed variability and slightly lower average pinch-off points follow.

Most modelled pinch-off points are below the observed points. A likely explanation for some of these cases is the spontaneous 'jumping' of the film from the inside to the outside of the tube wall at the tube opening. This can be seen in Figure 5.3. Adhesion between the tube bottom surface and the exiting water film sometimes causes the exiting film to 'jump' from the inner tube wall to the outer tube wall as it exits. This effectively increases

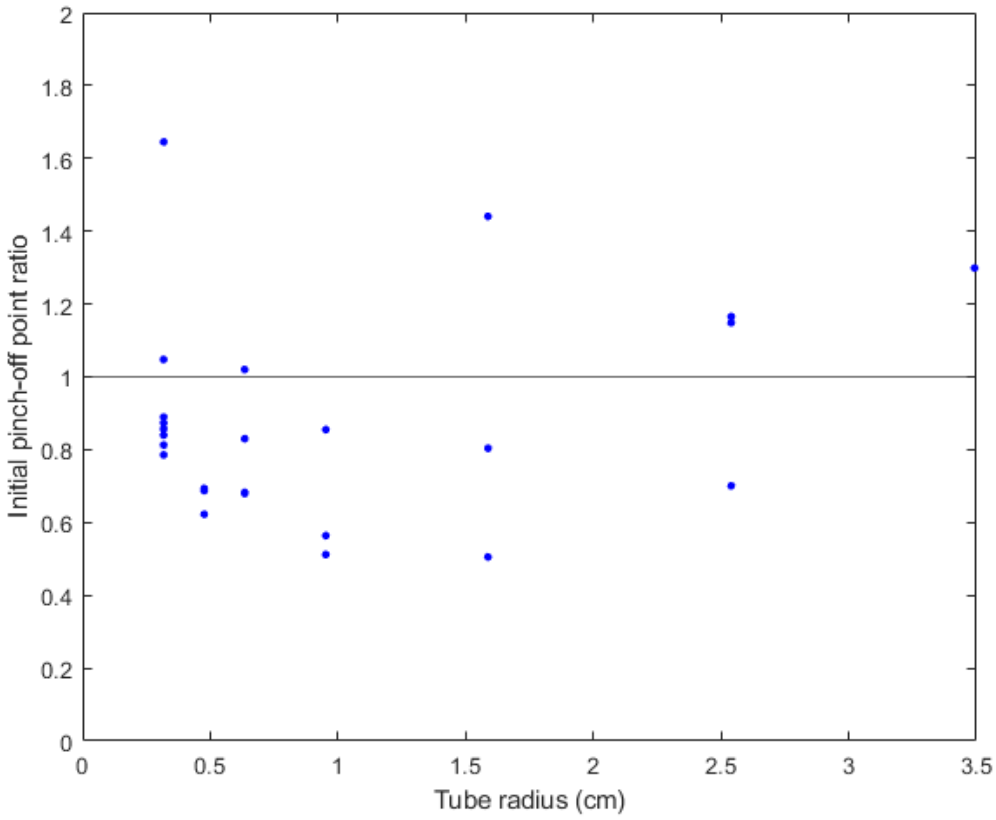

Fig. 5.2: Ratio of modelled vs. observed initial pinch-off points at various radii. All pinch-off points have a ratio between 0.5 and 1.65.

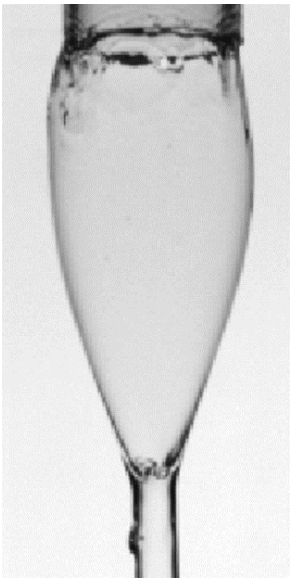

Fig. 5.3: Example of film after having 'jumped' to outside of tube wall. Adhesion from the tube draws the exiting film outward to the extent that the film outer surface is on the outer wall of the tube.

the initial water bell radius, which increases the observed pinch-off depth. This tends to happen in higher fill height and lower tube radius cases.

As discussed in Section 4.6, the cohesion of the water to itself can inhibit the water from pinching off at its theoretical point. This effect is mainly seen in the *Jumping champagne* behavior, but could also play a role in the average observed pinch-off being greater than the theoretical value. The cohesion of the water column to the film immediately above it could slow the rate of pinch off, creating a lower pinch-off point than the model calculates.

Finally, a possible reason for some of the variability seen between the model and observations is the delicate nature of the film. Because the film is only a fraction of a millimeter thick, it is very susceptible to vibrations on the tube or air disturbances. Though modest efforts were made to mitigate these disturbances (only testing when others are not walking by, etc.), some irregularities were occasionally observed, such as water bells being blown by

a small air disturbance. This may result in some variation in the observed pinch-off points.

CHAPTER 6

CONCLUSION

In conclusion, the behavior of water when suddenly allowed to descend out of a vertical tube was studied. Observations were collected across several tube diameters and water fill heights. A rich variety of interesting and beautiful water behaviors were observed, which were categorized into several regimes.

A model was derived that explains and predicts the observed behaviors using a variety of means, including first principle derivation, use of well-known existing models, and empirical correlations. The model includes analysis of pre-movement force interactions, accelerating water profile development inside the tube, entrained film drainage, film waviness development, and external falling film motion prediction (i.e. the water bell equations). These different equations and models, belonging to several separate areas of study, all interact to create the varied and fascinating range of behaviors observed. The model explains the reasons for the different film behaviors and reflects the observed data quite well.

This study has created a substantial groundwork that can be built upon in several potential directions in future work. For example, the equations and models derived here can easily be applied to fluids other than water. By using a different fluid with different surface tension, viscosity, and density values, it is anticipated that the predicted and observed behaviors could be quite different, with some behaviors disappearing and entirely new behaviors being observed. Another variable that could be changed is the tube contact angle. A highly hydrophobic tube, for example, would change pre-movement forces and

exiting water angle, which would potentially eliminate the *Static slug* and *Jet* behaviors could also have a large effect on external film behavior. Finally, new variables could be introduced, such as a background fluid with a more substantial effect on the fluid. Whereas air has very little effect on the water used in the study, an immiscible background fluid such as oil would both slow the drainage of the fluid in the tube and create substantial drag on the external film.

REFERENCES

[1] N. B. Speirs, J. Belden, Z. Pan, S. Holekamp, G. Badlissi, M. Jones, and T. T. Truscott, "The water entry of a sphere in a jet," *Journal of Fluid Mechanics*, vol. 863, pp. 956–968, 2019.

[2] N. B. Speirs, M. M. Mansoor, J. Belden, R. C. Hurd, Z. Pan, and T. T. Truscott, "Fluted films," *Physical Review Fluids*, vol. 3, p. 100504, Oct. 2018.

[3] Y. A. Çengel and J. M. Cimbala, *Fluid Mechanics: Fundamentals and Applications*. 1221 Avenue of the Americas, New York, NY 10020: McGraw-Hill, 3 ed., 2014.

[4] G. Szymanski, "Quelques solutions exactes des équations d'hydrodynamique du fluide visqueux dans le cas d'un tube cylindrique," *Journal de mathématiques pures et appliquées 9e série*, vol. 9, no. 11, pp. 67–108, 1932.

[5] P. J. Lefebvre, *Characterization of Accelerating Pipe Flow*. phdthesis, University of Rhode Island, 1987.

[6] P. Lefebvre and K. LaPointe, "Velocity profiles in constant-acceleration pipe flows," in *1st National Fluid Dynamics Conference*, p. 3752, 1988.

[7] J. K. Tapply, "Unsteady laminar fluid flow in the entrance region of a cylindrical pipe with a step change in pumping pressure," in *AIAA/ASME 4th Fluid Mechanics, Plasma Dynamics and Laser Conference*, vol. 86, (Atlanta, GA), p. 1039, AIAA/ASME, May 1986.

[8] L. Landau and B. Levich, "Dragging of a liquid by a moving plate," *Acta physicochimica U.R.S.S.*, vol. 17, no. 1-2, pp. 42–54, 1942.

[9] V. G. Levich, *Physicochemical Hydrodynamics*. Englewood Cliffs, N.J.: Prentice-Hall, 1962.

[10] G. C. Tallmadge, J.A., "Entrainment of liquid films: Drainage, withdrawal, and removal," *Industrial and Engineering Chemistry*, vol. 59, pp. 18–34, Nov. 1967.

[11] H. Jeffreys, "The draining of a vertical plate," *Mathematical Proceedings of the Cambridge Philosophical Society*, vol. 26, no. 2, pp. 204–205, 1930. cited By 87.

[12] C. Gutfinger and J. Tallmadge, "Some remarks on the problem of drainage of fluids on vertical surfaces," *AIChE Journal*, vol. 10, no. 5, pp. 774–780, 1964. cited By 31.

[13] J. Van Rossum, "Viscous lifting and drainage of liquids," *Applied Scientific Research, Section A*, vol. 7, no. 2-3, pp. 121–144, 1958.

[14] F. Goucher and H. Ward, "The thickness of liquid films formed on solid surfaces under dynamic conditions," *Phil. Mag*, vol. 44, pp. 1002–1014, 1922.

[15] A. Ali, A. Underwood, Y.-R. Lee, and D. Wilson, "Self-drainage of viscous liquids in vertical and inclined pipes," *Food and Bioproducts Processing*, vol. 99, pp. 38–50, 2016.

[16] G. Green, "Lvii. viscous motion under gravity in a liquid film adhering to a vertical plate," *The London, Edinburgh, and Dublin Philosophical Magazine and Journal of Science*, vol. 22, no. 148, pp. 730–736, 1936.

[17] G. Wyllie, "Lxx. drainage of a vertical plate," *The London, Edinburgh, and Dublin Philosophical Magazine and Journal of Science*, vol. 36, no. 259, pp. 581–585, 1945.

[18] N. Annapurna and G. Ramanaiah, "An inertial contribution to the steady state film profiles of viscous drainage," *Zeitschrift für Naturforschung A*, vol. 31, no. 8, pp. 1007–1008, 1976.

[19] S. Roy, "Inertia effects in laminar flow of thin liquid films," *Zeitschrift für angewandte Mathematik und Mechanik*, vol. 65, no. 11, pp. 578–579, 1985.

[20] C. D. Denson, "The drainage of newtonian liquids entrained on a vertical surface," *Industrial & Engineering Chemistry Fundamentals*, vol. 9, no. 3, pp. 443–448, 1970.

[21] K. Lang and J. Tallmadge, "A postwithdrawal expression for drainage on flat plates," *Industrial and Engineering Chemistry Fundamentals*, vol. 10, no. 4, pp. 648–650, 1971.

[22] D. de Kee, M. Schlesinger, and M. Godo, "Postwithdrawal drainage of different types of fluids," *Chemical Engineering Science*, vol. 43, no. 7, pp. 1603–1614, 1988.

[23] P. Kapitza and S. Kapitza, "Wave flow of thin fluid layers of liquid," *Zh. Eksp. Teor. Fiz*, vol. 19, p. 105, 1949.

[24] R. Camassa, H. R. Ogrosky, and J. Olander, "Viscous film flow coating the interior of a vertical tube. part 1. gravity-driven flow," *Journal of Fluid Mechanics*, vol. 745, pp. 682–715, Apr. 2014.

[25] H. R. Ogrosky, *Modeling Liquid Film Flow Inside a Vertical Tube*. PhD thesis, University of North Carolina at Chapel Hill, 2013.

[26] J. Muñoz-Cobo, S. Iglesias, D. S. Dominguez, A. Escrivá, and C. Berna, "Analytical model and numerical stability analysis for falling liquid film regimes in vertical pipes,"

in *10th Conference on Multiphase flow*, vol. 123, pp. 89–100, WIT Transactions on Engineering Sciences, July 2019.

[27] L. T. Nguyen and V. Balakotaiah, "Modeling and experimental studies of wave evolution on free falling viscous films," *Physics of Fluids*, vol. 12, no. 9, pp. 2236–2256, 2000.

[28] Y. Koizumi, R. Enari, and H. Ohtake, "Correlations of wave characteristics for a liquid film falling down along a vertical wall," *Journal of heat transfer*, vol. 131, no. 8, 2009.

[29] A. Ito and M. Sasaki, "Breakdown and formation of a liquid film flowing down an inclined plane," *Trans. Jpn. Soc. Mech. Eng*, vol. 52, pp. 1261–1265, 1986.

[30] H. Takahama and S. Kato, "Longitudinal flow characteristics of vertically falling liquid films without concurrent gas flow," *International Journal of Multiphase Flow*, vol. 6, no. 3, pp. 203–215, 1980.

[31] T. Takamasa and K. Kobayashi, "Measuring interfacial waves on film flowing down tube inner wall using laser focus displacement meter," *International Journal of Multiphase Flow*, vol. 26, no. 9, pp. 1493–1507, 2000.

[32] F. Savart, "Memoire sur la constitution des veines liquides lancées par des orifices circulaires en mince paroi," *Annales de chimie*, vol. 54, pp. 56–87, 1833.

[33] F. Savart, "Suite du memoire sur le choc d'une veine liquide lancee contre un plan circulaire," *Annales de chimie*, vol. 54, pp. 113–145, 1833.

[34] F. Savart, "Memoire sur le choc de deux veines liquides animees de mouvements directementopposes," *Annales de chimie*, vol. 55, pp. 257–310, 1833.

[35] M. E. Bourdon, "Water bells," *Nature*, vol. 30, no. 774, pp. 408–409, 1884.

[36] J. Boussinesq, "Theories des experiences de savart, sur la forme que prend une veine liquideapres s'être choquee contre un plan circulaire," *C. R. Acad. Sci. Paris*, vol. 69, pp. 45–48, 1869.

[37] J. Boussinesq, "Theories des experiences de savart, sur la forme que prend une veine liquideapres s'être heurtee contre un plan circulaire (suite)," *C. R. Acad. Sci. Paris*, vol. 69, pp. 128–131, 1869.

[38] E. Buchwald and H. König, "Über wasserglocken," *Annalen der Physik*, vol. 415, no. 6, pp. 557–569, 1935.

[39] E. Buchwald and H. König, "Dynamische oberflächenspannung aus flüssigkeitsglocken," *Annalen der Physik*, vol. 418, no. 7, pp. 659–672, 1936.

[40] W. Bond, "The surface tension of a moving water sheet," *Proceedings of the Physical Society*, vol. 47, no. 4, p. 549, 1935.

[41] H. Puls, "Lxxxii. the surface tension of a moving mercury sheet," *The London, Edinburgh, and Dublin Philosophical Magazine and Journal of Science*, vol. 22, no. 150, pp. 970–982, 1936.

[42] F. L. Hopwood, "Water bells," *Proceedings of the Physical Society. Section B*, vol. 65, no. 1, p. 2, 1952.

[43] G. N. Lance and R. L. Perry, "Water bells," *Proceedings of the Physical Society. Section B*, vol. 66, p. 1067, Dec. 1953.

[44] S. G. Taylor, "The dynamics of thin sheets of fluid. i. water bells," *Proceedings of the Royal Society, Section A*, vol. 253, Dec. 1959.

[45] G. I. Taylor, "The dynamics of thin sheets of fluid. iii. disintegration of fluid sheets," *Proceedings of the Royal Society of London. Series A. Mathematical and Physical Sciences*, vol. 253, no. 1274, pp. 313–321, 1959.

[46] J.-Y. Parlange, "A theory of water-bells," *Journal of Fluid Mechanics*, vol. 29, pp. 361–372, Aug. 1967.

[47] J. Dumbleton, "Effect of gravity on the shape of water bells," *Journal of Applied Physics*, vol. 40, no. 10, pp. 3950–3954, 1969.

[48] C. Clanet, "Stability of water bells generated by jet impacts on a disk," *Physical Review Letters*, vol. 85, no. 24, pp. 1506–5109, 2000.

[49] C. Clanet, "Dynamics and stability of water bells," *Journal of Fluid Mechanics*, vol. 430, pp. 111–147, Mar. 2001.

[50] J. M. Aristoff, C. Lieberman, E. Chan, and J. W. M. Bush, "Water bell and sheet instabilities," *Physics of Fluids*, vol. 18, p. 091109, Sept. 2006.

[51] P. Brunet, C. Clanet, and L. Limat, "Transonic liquid bells," *Physics of Fluids*, vol. 16, pp. 2668–2678, July 2004.

[52] G. J. Jameson, C. E. Jenkins, E. C. Button, and J. E. Sader, "Water bells formed on the underside of a horizontal plate. part 1. experimental investigation," *Journal of fluid mechanics*, vol. 649, pp. 19–43, 2010.

[53] E. C. Button, J. F. Davidson, G. J. Jameson, and J. E. Sader, "Water bells formed on the underside of a horizontal plate. part 2. theory," *Journal of fluid mechanics*, vol. 649, pp. 45–68, 2010.

[54] F. D. Petke and B. R. Ray, "Temperature dependence of contact angles of liquids on polymeric solids," *Journal of Colloid and Interface Science*, vol. 31, no. 2, pp. 216–227, 1969.

[55] K. Terpilowski, D. Rymuszka, L. Holysz, and E. Chibowski, "Changes in wettability of polycarbonate and polypropylene pretreated with oxygen and argon plasma," 2014.